Cuaternario y Geomorfología
ISSN: 0214-1744
ISSNe: 2695-8589

www.rediris.es/CuaternarioyGeomorfologia/

Los Villares locality (Ruidera, Castilla-La Mancha, Spain): a new Middle Pleistocene fossil assemblage from the Southern Iberian Plateau with possible evidence of human activity

Yacimiento de los Villares (Ruidera, Castilla-La Mancha, España): un nuevo conjunto fósil del Pleistoceno Medio en la Submeseta Sur Ibérica con posible evidencia de actividad antrópica

García-Martínez, D.[(1), (2), (3), (4)]*; Duval, M.[(2), (5)]; Zhao, J.-X.[(6)]; Feng, Y.[(6)]; Wood, R.[(7)], Huguet, R.[(8), (9), (10)], Cifuentes-Alcobendas, G. [(11), (12)]; Palancar, C. A.[(4)]; Moya-Maleno, P.R. [(3), (13)]

[(1)] Physical Anthropology Unit, Department of Biodiversity, Ecology, and Evolution, Faculty of Biological Sciences, Complutense University of Madrid, Madrid, Spain. Email: dangar29@ucm.es
[(2)] Centro Nacional de Investigación sobre la Evolución Humana (CENIEH), Paseo Sierra de Atapuerca, 3, 09002 Burgos, Spain.
[(3)] Centro de Estudios del Campo de Montiel (CECM), Plaza Mayor s/n, 13328 Almedina, Castilla-La Mancha, Spain.
[(4)] Paleoanthropology Group, Museo Nacional de Ciencias Naturales (CSIC), José Gutiérrez Abascal 2, 28006 Madrid, Spain.
[(5)] Australian Research Centre for Human Evolution (ARCHE), Griffith University, Nathan, QLD 4111, Australia.
[(6)] Radiogenic Isotope Facility, School of Earth and Environmental Sciences, The University of Queensland, Brisbane, QLD 4072, Australia.
[(7)] Research School of Earth Sciences, Australian National University, Building 142 Mills Road, Acton, ACT 2601, Australia.
[(8)] IPHES-CERCA, Insitut Català de Paleocologia Humana i Evolució Social, Zona Educacional, 4, Campus Secelades URV (Edifici W3) E3, 43700 Tarragona, Spain.
[(9)] Departament d'Historia i Historia de l'Art. Universitat Rovira i Virgili (URV). Avinguda de Catalunya, 35, 43002, Tarragona, Spain
[(10)] Unit associated to CSIC. Departamento de Paleobiología, Museo Nacional de Ciencias Naturales, c/ José Gutiérrez Abascal 2, 28006 Madrid, Spain.
[(11)] IDEA (Institute of Evolution in Africa), University of Alcalá de Henares, Covarrubias 36, 28010, Madrid, Spain.
[(12)] Area of Prehistory, Department of History and Philosophy, University of Alcalá de Henares, C/ Colegios 2, 28801 Alcalá de Henares, Madrid, Spain
[(13)] Área de Prehistoria, Facultad de Geografía e Historia, Complutense University of Madrid, c/Profesor Aranguren S/N, 28040 Madrid, Spain.

*** Corresponding author.**

https://doi.org/10.17735/cyg.v36i1-2.90422

Summary

We present the discovery of a Middle Pleistocene fossil assemblage at Los Villares locality (Ruidera, Ciudad Real, Castilla-La Mancha), which has possible evidence of associated human activity. The potential of the site has been evaluated through multidisciplinary research including taxonomy, anatomy, deep learning, and direct dating of fossil remains. A surface study carried out in 2017, over a very limited area (2 m^2) on the slope of one of the Ruidera lakes led to the discovery of more than 50 fossil specimens, including cranial (mainly teeth) and postcranial remains. This rich assemblage is dominated by the remains of Caprinae, although the presence of some small or medium carnivore remains also stands out. The identification of a cut mark, tested with Convolutional Neural Networks, suggests the presence of human activity within the bone assemblage. Several fossils were directly dated using a multi-technique approach involving radiocarbon, U-Th, and ESR methods. The results constrain the fossil assemblage to between 300 ka and 400 ka, positioning Los Villares as one of the first Middle Pleistocene localities identified in the Upper Guadiana basin, on the Southern edge of the Southern Iberian Plateau. These promising initial results show the great potential of the site to contribute to filling a gap of knowledge in the Pleistocene archaeo-paleontological record of the Iberian Peninsula. Nevertheless, we also acknowledge the need for systematic excavations in the future, not only to obtain a better idea of the lateral and stratigraphic extension of the fossil assemblage and its complete taxonomic composition, but also to confirm the human presence at the site.

Key words: paleontology; Southern Iberian Plateau; Middle Pleistocene; direct dating; taphonomy; cut mark.

Resumen

Presentamos aquí el descubrimiento de un conjunto fósil del Pleistoceno Medio encontrado en Los Villares (Ruidera, Ciudad Real, Castilla-La Mancha), con posible evidencia asociada de actividad humana. El potencial del yacimiento ha sido evaluado a través de una investigación multidisciplinaria que incluye anatomía, *Deep learning* y datación directa de restos fósiles. Un estudio de los materiales superficiales, donados recientemente y procedentes de un área muy limitada (2 m^2) en la ladera de una de las lagunas de Ruidera, condujo al descubrimiento de más de 50 especímenes fósiles, incluidos restos craneales (principalmente dientes) y postcraneales. Este rico conjunto está dominado por restos de Caprinae, aunque también destaca la presencia de algún resto de pequeño o mediano carnívoro. La identificación de una marca de corte, testada con técnicas estadísticas utilizando Redes Neuronales (*Convolutional Neural Networks*), en un resto pone de manifiesto la presencia de actividad antrópica en el conjunto. Además, varios fósiles fueron datados directamente por medio de un enfoque de múltiples técnicas que involucran métodos de Radiocarbono, U-Th y ESR, proporcionando un rango cronológico de entre 300 ka y 400 ka para los fósiles. Este es, que sepamos, uno de los primeros yacimientos fechados del Pleistoceno medio en la Meseta del Sur de la Península Ibérica, especialmente en la cuenca alta del Río Guadiana. Estos prometedores resultados iniciales demuestran el gran potencial de la localidad de Los Villares para contribuir a llenar un vacío de conocimiento en el registro arqueológico-paleontológico del Pleistoceno Medio de la Península Ibérica. No obstante, reconocemos la necesidad de realizar excavaciones sistemáticas en el futuro para tener no solo una mejor idea de las extensiones laterales y estratigráficas, así como de la composición taxonómica del conjunto fósil, sino también para confirmar la presencia humana en el sitio.

Palabras clave: paleontología; Submeseta Sur Ibérica; Pleistoceno medio; datación directa; tafonomía; marca de corte.

1. Introduction

The Iberian Peninsula is characterized by an abundant and diverse Pleistocene archeo-paleontological record, with fossil assemblages mostly found in karstic (caves, chambers, or shelters), fluvial (river channels or floodplains), and marshy or lacustrine environments (Arribas Herrera & Jordá Pardo, 1999; Jordá Pardo, 2008a). While these localities cover the entire Peninsula, they are mostly concentrated in several geological units (Jordá Pardo, 2008b) in both mountainous areas such as the Cantabrian Mountains and the Pyrenees, the Central System, the Iberian, and Coastal-Catalan Ranges and the Baetic System, and the major river basins of the Tagus, Guadiana (including the Campo de Calatrava sub-basin) and Guadix-Baza. However, whilst Middle Pleistocene fossil deposits are frequent in these mountainous regions, only the Guadix-Baza basin contains numerous large mammal assemblages, and sites in the two basins (the Tagus and Guadiana Basins) in the "Southern Iberian Plateau" are much less proliferous, leaving a substantial gap in the record.

For example, in the Cantabrian Mountains and Pyrenees, El Sidrón (Rosas *et al*., 2012), El Castillo (Valdés, 1984) and Lezetxiki (Baldeón, 1993) have yielded significant Pleistocene assemblages of faunal and human remains, as have, Pinilla del Valle (Baquedano *et al*., 2012) and Jarama VI (Jordá Pardo, 2007) in the Central System and the Atapuerca karst complex (Arsuaga *et al*., 1999; Bermúdez de Castro *et al*., 1997), Torralba and Ambrona sites (Falguères *et al*., 2006), Cueva de los Casares (Barandiarán & Altuna, 1973) and Cova de Bolomor (Fernández Peris *et al*., 2008) in the Iberian and Coastal-Catalan Ranges. Similarly, among the three basins mentioned by Jordá Pardo (2008b?), the Guadix-Baza is represented by a substantial number of fossil sites including Fonelas P-1 (Arribas Herrera *et al*., 2001), Solana del Zamborino (Álvarez-Posada *et al*., 2017), and the Orce archaeo-paleontological complex (Arribas Herrera & Palmqvist, 1998; Titton *et al*., 2020; Toro-Moyano *et al*., 2013). In contrast, the Tagus and Guadiana basins in the "Southern Iberian Plateau" are much less proliferous. The Tagus Basin is represented by fossil sites such as Áridos (Blain *et al*., 2014; Santonja *et al*., 2001), TAFESA (Sesé, 2010), or Perales del Río (Sesé & Soto, 2002) and Jordá Pardo (2008a) lists only Pliocene fossil sites such as Las Higueruelas in the Upper Guadiana basin. This reflects a real bias in the archeo-paleontological record of the Southern Iberian Plateau, and more specifically in the Upper Guadiana Basin (García-Martínez, 2019).

In this context, the discovery of a new Pleistocene fossil assemblage at Los Villares, i.e. within the Upper Guadiana basin in the Southern Plateau, is of particular interest. Here we report the initial results from a multidisciplinary investigation including taxonomy, taphonomy, and geochronology designed to evaluate the potential of Los Villares.

1.1. Context

1.1.1. Overview of the evidence of the human presence in the Iberian Peninsula during the Middle Pleistocene

While the Early Pleistocene archaeological and fossil record of the Iberian Peninsula is quite rich and diverse, it shows a significant hiatus from the end of the Early Pleistocene to around 500 ka, well into the Middle Pleistocene, where there is little evidence to support the presence of hominin species. Around 500-400 ka, a human species very different to the earlier *Homo antecessor*, both in terms of body size and shape (Arsuaga *et al*., 1999, 2015; Carretero *et al*., 2004) and associated typo-technological assemblages (Ollé *et al*., 2013), has been well documented in Atapuerca (Sima de Los Huesos and Gran Dolina TD10) and Gruta de Aroeira (Daura *et al*., 2017) at the end of the Tagus Basin (Portugal). This species, now considered as "pre-Neanderthal" (Arsuaga *et al*., 2014), produced a Mode 2 technology associated with systematic and directional carcass processing, includ-

ing hunting events like in Gran Dolina TD10 (García-Medrano *et al*., 2015; Rodriguez-Hidalgo *et al*., 2017). The rest of the Middle and Late Pleistocene is well documented by the presence of Neanderthals in the Iberian Peninsula, with Mode 3 technology and numerous fossil sites all around the Iberian Peninsula (Baquedano *et al*., 2012; Fernández Peris *et al*., 2008; Rodriguez-Perez *et al*., 2017; Rosas *et al*., 2006; Rosas *et al*., 2017; Walker *et al*., 2011). However, whilst the Iberian Peninsula is characterized by an overall dense and diverse Early-to-Late Pleistocene archaeological and fossil record, the Southern Plateau, and the Guadiana Basin, in particular, is clearly contrasting with the big picture, with only few Middle Pleistocene archeo-paleontological localities identified so far.

1.1.2. The Plio-Pleistocene fossil record from the Southern Plateau and the Guadiana Basin

The Southern Plateau (*Meseta sur*) of the Iberian Peninsula is an extended plain of moder-

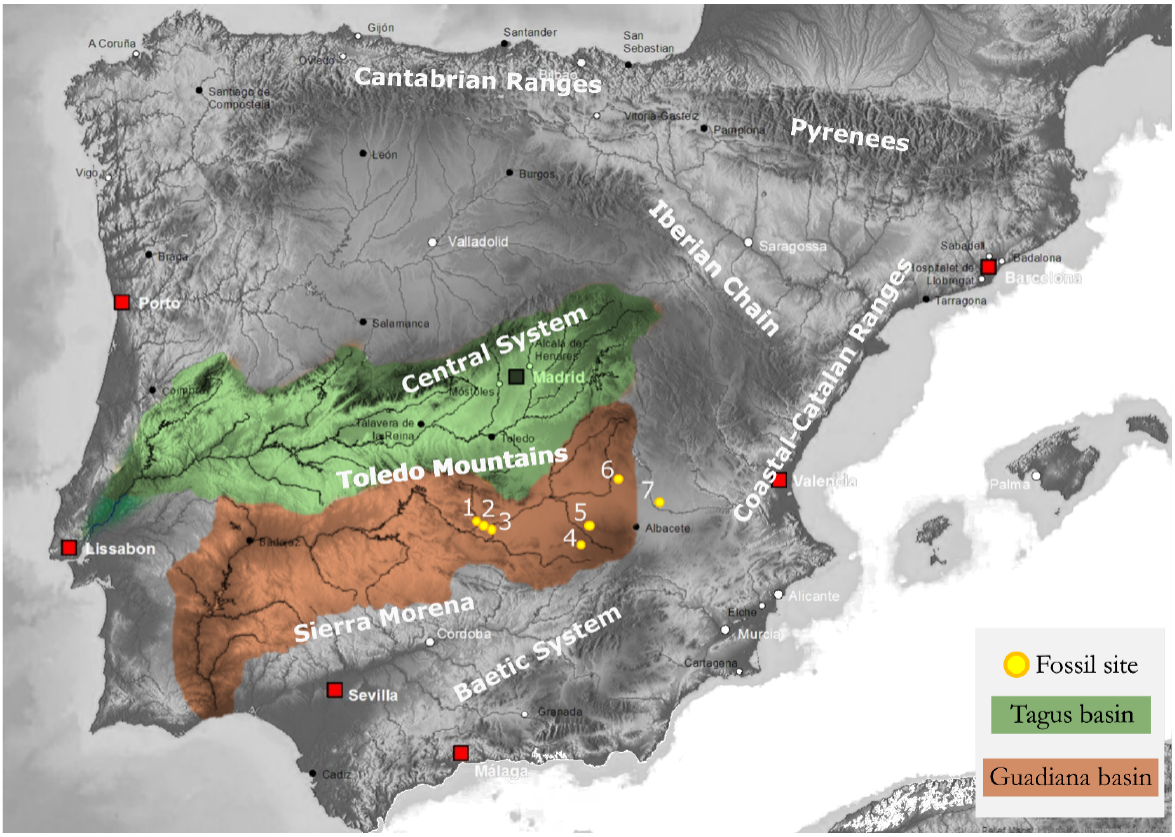

Figure 1: Geographical setting of the Tagus (green) and Guadiana (brown) Basins. The main fossil sites identified in the Upper Guadiana basin (yellow circles) are highlighted. 1: Bonete y Piedrabuena (Pliocene); 2: Las Higueruelas (Pliocene); 3: Valverde de Calatrava I (Lower to Middle Pleistocene) y II (Pliocene); 4: Cueva de los Toriles (Middle Pleistocene); 5: Los Villares (Middle Pleistocene); 6: El Provencio (Middle Pleistocene); 7: Fuensanta del Júcar (Lower to Middle Pleistocene). Modified from https://commons.wikimedia.org/, CC BY-SA 3.0.

Figura 1: Marco geográfico de las cuencas del Tajo (verde) y Guadiana (marrón). Se destacan los principales yacimientos fósiles identificados en la cuenca del Alto Guadiana (círculos amarillos). 1: Bonete y Piedrabuena (Plioceno); 2: Las Higueruelas (Plioceno); 3: Valverde de Calatrava I (Pleistoceno Inferior a Medio) y II (Plioceno); 4: Cueva de los Toriles (Pleistoceno Inferior a Medio); 5: Los Villares (Pleistoceno Medio); 6: El Provencio (Pleistoceno Medio); 7: Fuensanta del Júcar (Pleistoceno Inferior a Medio). Modificado de https://commons.wikimedia.org/, CC BY-SA 3.0.

ate altitude (mostly around 600-700 m.a.s.l.) compared with its Northern part, which is dissected by the present-day fluvial networks of the Tagus and Upper Guadiana rivers (Fig. 1). It is bordered by mountain ranges such as the Central System (to the North), the Iberian Chain (to the Northeast), and the Baetic System, and Sierra Morena (to the South) (Casas-Sainz & de Vicente, 2009). The geography of this area is characterized by large plain terrains along the Tagus and Guadiana basins, except for the Toledo Mountains area, which roughly separates the two basins. From a geological point of view, the easternmost part of the Southern Plateau is mainly composed of Neogene and Quaternary deposits, except for some islets within the Campo de Montiel area which are formed by large limestone plaques from the Mesozoic era and settled on much folded Paleozoic substrates giving rise to more rugged landscapes (Casas-Sainz & de Vicente, 2009; de la Cruz, 2013; Montero González, 2003; Jiménez Ramírez & Chaparro Sabina, 1989; Ramírez *et al*., 1982). In the westernmost part of the Southern Plateau, Precambrian-Paleozoic substrates are most common (Casas-Sainz & de Vicente, 2009). Given these geological and geographical features, Plio-Pleistocene fossil assemblages identified in the region are found mostly associated with either the fluvial deposits of the Tagus and Upper Guadiana basins or the karstic sedimentary infilling systems in the easternmost part (García-Martínez, 2019).

Focusing on the Guadiana Basin, a few and relatively unexplored Pliocene localities have been described in the literature, such as Las Higueruelas (Badiola *et al*., 2007), Bonete y Piedrabuena (Torres & Mazo, 1991) and Valverde de Calatrava II (Alberdi *et al*., 1984), both in the Campo de Calatrava area (Fig. 1). Their Pliocene chronology has been mostly inferred from biochronology. Lower-to-Middle Pleistocene localities have been also reported, such as Valverde de Calatrava I, Fuensanta del Júcar and El Provencio (Domínguez-Solera *et al*., 2020; Mazo *et al*., 1990) (Fig. 1). The latter two were found in fluvial deposits associated with the Júcar and Záncara Rivers, in terraces positioned +60 m and +15-16 m above the current river channel, respectively, and belonged to the Guadiana fluvial network during Pleistocene times (Mazo *et al*., 1990; Santisteban & Schulte, 2007). Based on the identification of the large mammal taxa *Mammuthus meridionalis* or *Hippopotamus amphibius major* at Valverde de Calatrava I and Fuensanta del Júcar, age estimates of around 1.3-0.8 Ma (Aguirre, 1989; Mazo, 1999) and 1 Ma (Mazo *et al*., 1990) were inferred respectively. The archeo-paleontological site of El Provencio (Cuenca) provided fossil remains initially attributed to *Mammuthus meridionalis,* suggesting a similar Lower Pleistocene chronology to the Fuensanta del Júcar assemblage (Mazo *et al*., 1990). However, a Middle Pleistocene age is more likely as a recent study suggested that these remains could be instead attributed to *Mammuthus trogontherii*, a species covering a younger time range, and one ESR date obtained from the lowermost and sterile stratigraphic unit provides a burial age of around 800 ka (Domínguez-Solera *et al*., 2020). Finally, García-Martínez *et al*. (2020) and Megía García *et al*. (2020) recently reported the discovery of a fossil assemblage and associated Middle Paleolithic lithic tools at the cave site of Cueva de Los Toriles (Carrizosa, Castilla-La Mancha) (Fig. 1), with a potential Middle Pleistocene chronology (unpublished data).

1.2. Los Villares locality

In April 2009, P.R.M.M. was informed of the discovery of bone fragments on one of the slopes of the Los Villares house state, located on the "La Colgada" lake, on the right bank of the *Parque Natural de las Lagunas de Ruidera* (Ciudad Real, Castilla-La Mancha) (Fig. 2). It was not until a decade later that a multidisciplinary team was able to gather and provide the first formal evaluation of this new site, which is presented here for the first time to the scientific community.

The Ruidera lakes are a series of 14 lakes dammed with tuff barriers along ~15 km of a

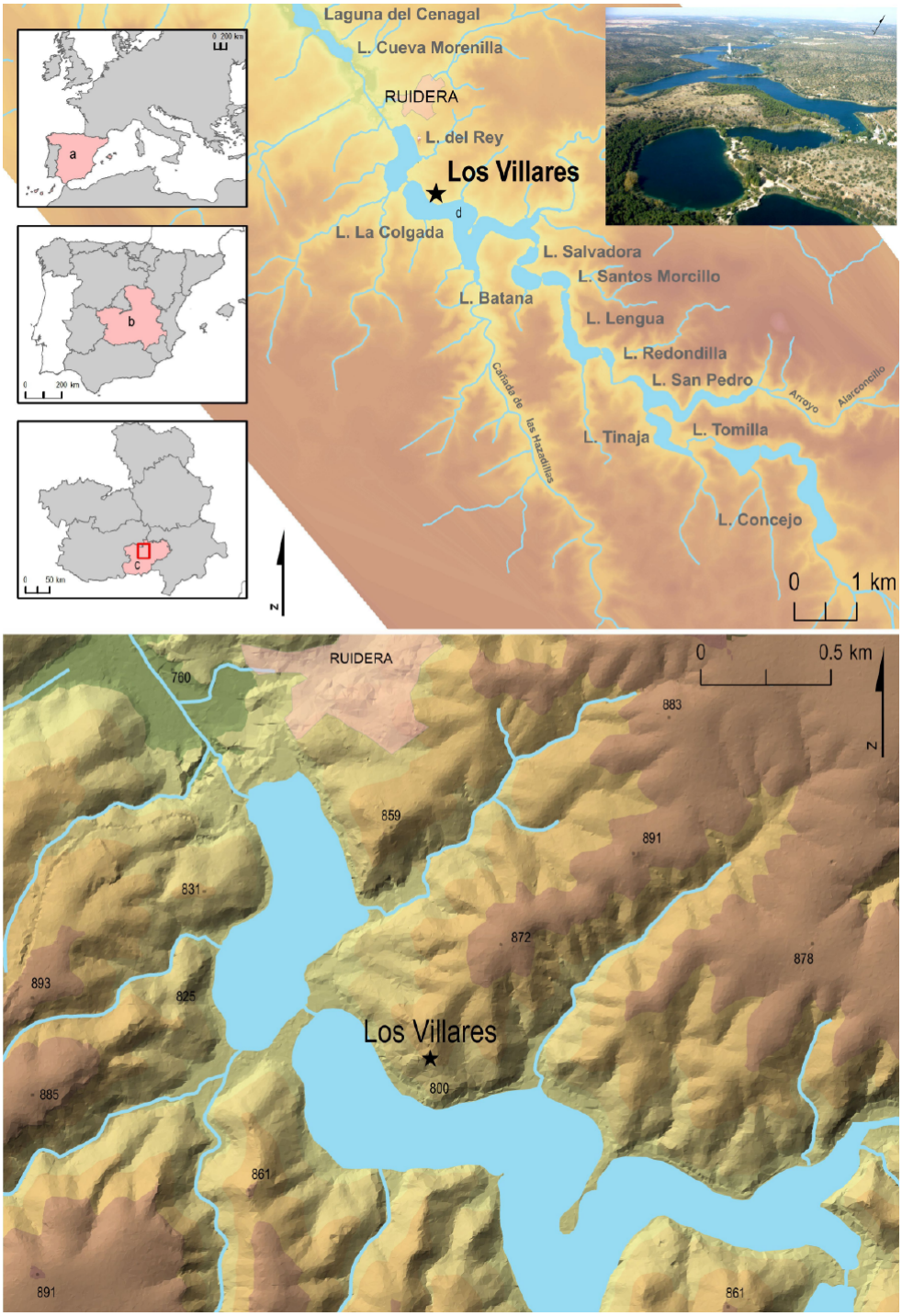

Figure 2: Geographical setting of Los Villares locality (Ruidera, Ciudad Real, Castilla-La Mancha). Legend: a) Spain, b) Castilla-La Mancha province, c) Campo de Montiel area. Built with QGIS 3.12.3 -GNU Free License- and free wms data from Instituto Geográfico Nacional (IGN), Spain).

Figura 2: Marco geográfico de la localidad de Los Villares (Ruidera, Ciudad Real, Castilla-La Mancha). Leyenda: a) España, b) Provincia de Castilla-La Mancha, c) Zona de Campo de Montiel. Construido con QGIS 3.12.3 -GNU Free License- y datos wms gratuitos del Instituto Geográfico Nacional (IGN), España).

Figure 3: Fossiliferous sediments exposed after a road construction at the house state of Los Villares (Ruidera, Ciudad Real), in 2009.

Figura 3: Sedimentos fosilíferos expuestos tras la construcción de una carretera en la urbanización Los Villares (Ruidera, Ciudad Real), en 2009.

headwater of the Guadiana River, that incise the Mesozoic carbonates forming the high plateau of *Campo de Montiel* (Ordóñez *et al*., 2005, González Martín *et al*. (1987) in the southern part of the Southern Plateau. This exceptional karstic landcape, is similar to the Plitvice lakes in Croatia, mentioned in Roman times (Álvarez *et al*., 2007; González Martín, 2007; González Martín *et al*., 2004; Planchuelo, 1952), and has important natural resources such as fish farms, game animals and perpetual pastures (Moya-Maleno, 2011).

The current morphology of the lakes dates from the Holocene, around 6,000 years ago (González Martín *et al*., 1987; Montero González, 2003). However, geomorphological studies suggest the constant transformation of the area over time, both by natural episodes, such as the earthquake of the 16th century, and human action (Hijano, 2013; López Sanz, 1993; Martín, 2000), leading to modification and, sometimes, the disappearance of some lakes (Álvarez *et al*., 2007; Marín Magaz, 2007).

The paleontological site of Los Villares is located on the eastern slope above the La Colgada lake at 808 meters above sea level (m.a.s.l.), i.e. about 21 meters above the current lake level (787 m.a.s.l.) and about 80 meters from the shore on a 45º slope. During the construction of a local road, more than 50 excellently-preserved faunal fossils were identified and surface-collected in 2017 by locals from an area of about 2 m^2 (Fig. 3).

2. Material and methods

2.1. Fossil assemblage

Anatomical and taxonomic identifications of all fossil remains recovered from Los Villares (N=57) were based on the comparative material collections from the Museo Nacional de Ciencias Naturales (MNCN-CSIC). Of the 57 elements, 53 were clean and individualized (Figs. 4, 5), while three were still embedded in breccia (Fig. 6). The last specimen was only studied through pictures since it was recovered in 2009 and access to the original fossil could not be obtained (Fig. 7).

2.2. Preliminary taphonomic study

First, we analyzed the breakage pattern of the bones using the Villa and Mahieu model (Villa & Mahieu, 1991). In addition, the surface of the bones was inspected with a binocular magnifier to identify and describe potential marks resulting from human activity. Once identified, we carried out a deep learning approach to confirm their human origin.

To accurately identify the type of taphonomical alteration (i.e., cut mark, tooth mark, trampling mark, etc.) present in the specimen, an approach combining deep learning and computer vision was employed. Deep learning and

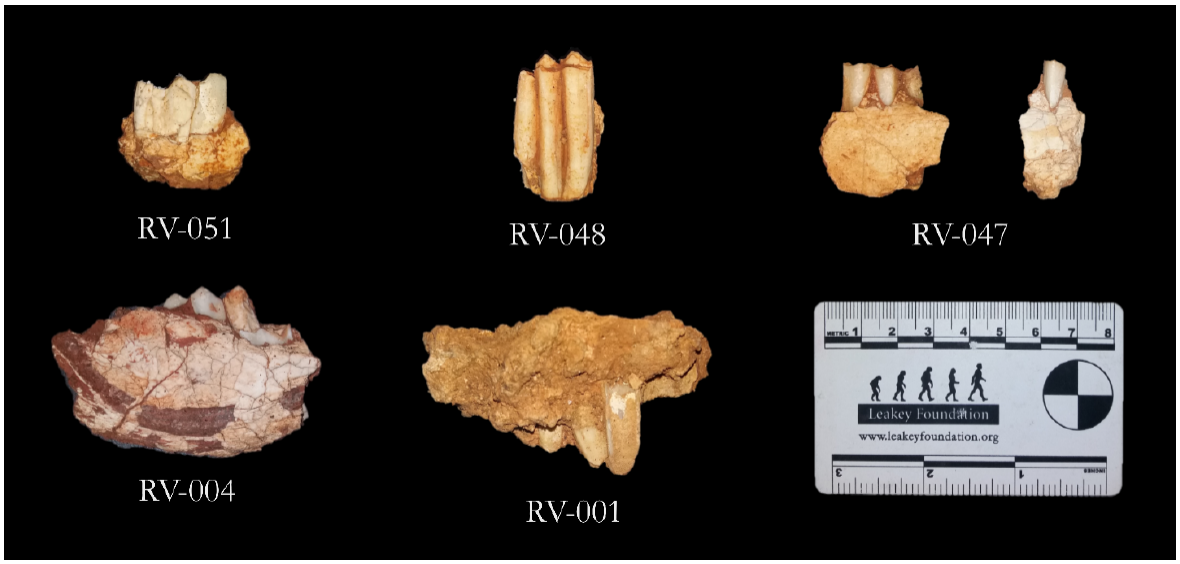

Figure 4: Examples of dental fossil remains recovered from Los Villares locality (see descriptions in Table 5).
Figura 4: Ejemplos de restos fósiles dentales recuperados en la localidad de Los Villares (ver descripción en la Tabla 5).

Figure 5: Examples of skeletal elements recovered from Los Villares locality (see descriptions in Table 5).
Figura 5: Ejemplos de elementos óseos recuperados en la localidad de Los Villares (ver descripción en Tabla 5).

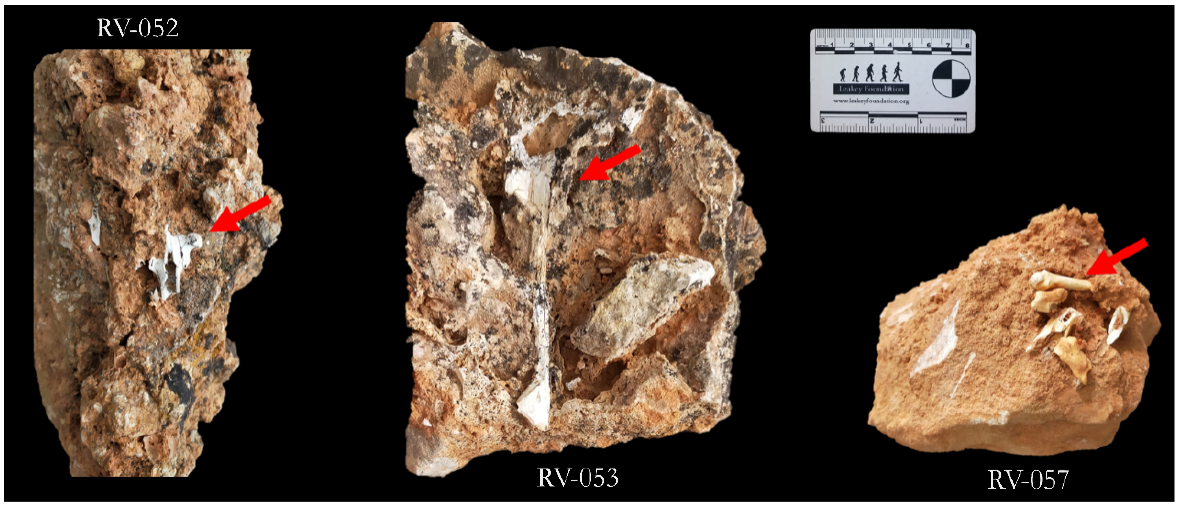

Figure 6: Examples of brecciated fossil specimens (red arrow) recovered from Los Villares locality (see descriptions in Table 5).

Figura 6: Ejemplos de especímenes fósiles brechificados (flecha roja) recuperados de la localidad de Los Villares (ver descripciones en la Tabla 5).

Figure 7: Felinae mandible recovered from Los Villares locality. Only pictures could be studied from this specimen since we did not have access to the original specimen (see descriptions in Table 5).

Figura 7: Mandíbula de Felinae recuperada de la localidad de Los Villares. Solo se pudieron estudiar fotografías de este espécimen ya que no tuvimos acceso al espécimen original (ver descripciones en la Tabla 5).

Computer Vision algorithms based on Convolutional Neural Networks (CNN) have recently been successfully used to classify different types of bone surface modifications (e.g., (Byeon *et al*., 2019; Cifuentes-Alcobendas & Domínguez-Rodrigo, 2019; Domínguez-Rodrigo *et al*., 2020). These algorithms have been able to outperform human analysts in accuracy rates while providing more replicable results and more objectivity than previous methods (Domínguez-Rodrigo *et al*., 2020). Here, we used transfer learning to guarantee optimal feature extraction of the models with relatively small sample sizes. The models used were both with sequential (VGG16 and VGG19) and parallel (ResNet50, DenseNet201, and InceptionV3) architectures, and their accuracy rates ranged from 89% to 92% in our preliminary tests. The reader may refer to Domínguez-Rodrigo *et al*. (2020) (ResNet50, VGG16, VGG19, and InceptionV3 models) and Abellán *et al*. (2021) (DenseNet201) for more information on Artificial Intelligence model building and tuning. Additionally, we selected a Rectified Linear Unit (ReLU) as the activation function and a Stochastic Gradient Descent (SGD) as an optimizer, since these two have become the baseline of CNNs for their efficiency and good overall performance (Goodfellow *et al*., 2016; Ketkar, 2017).

These models were trained on a mixed sample of images of cut marks (N=488), tooth marks (N=106), and trampling marks (N=63). The images were taken at x30 magnification using a binocular microscope, then turned to grayscale and trimmed to show only the inner groove and shoulders of the marks. Augmentation techniques (i.e., rotation, skewing, horizontal and vertical translation, and mirroring) were used to increase sample variance, avoid overfitting, and improve the model performance when subjected to images not used during the training (Ketkar, 2017). Models were trained on batches of 32 images of 80x400 pixel resolution (.bmp format) updating the weights with backpropagation for 100 epochs each. The coding and training of the models were undertaken in Tensorflow (v. 2.3.0) and Keras (v. 2.4.3), in a Conda environment capable of CUDA computing with cuDNN (v. 11.2) (Chetlur *et al*., 2014).

2.3. Characterization of the sediment

One sample of breccia attached to tooth RV-001 was collected for laboratory characterization analyses at CENIEH: grain size analysis was performed using the Robinson pipette method, and X-ray Fluorescence (XRF) was used to obtain some insights into the composition of the sediment in major elements.

2.4. Direct dating

2.4.1. Samples

Several fossil specimens were collected *in situ* and selected for dating purpose, following a multi-technique approach combining Radiocarbon (#546, #548 & #549), U-series (#546, #547 & #548) and Electron Spin Resonance (ESR) (#546) (Table 1).

2.4.2. Radiocarbon dating

The nitrogen percentage (%N) in both bone (#546, #548, and #549) and dentine (#548) was measured to establish whether sufficient collagen for radiocarbon dating was present. After removing the soft surface, 2-5 mg of bone/dentine powder was collected with a handheld Dremel™ drill and measured using an ANCA elemental analyzer connected to a Sercon 20-22 isotope ratio mass spectrometer operating in continuous flow mode, using an in-house gelatine reference. Analyses were performed at the Australian National University (ANU) Radiocarbon Laboratory, Australia.

2.4.3. U-series dating

Laser ablation (LA) and Solution U-series analyses were carried out using a Nu Plasma HR MC-ICP-MS in the Radiogenic Isotope Facility (RIF) at the School of Earth and Environmental Sciences, the University of Queensland (Australia).

Laser ablation MC-ICP-MS U-series dating: The LA analyses were carried out on tooth fragments collected from samples #546, #547, and #548 following the principles and procedures modified after Grün *et al*. (2014). Rather than applying off-line reduction of raw isotope signal intensity data to calculate the sample's $^{230}Th/^{238}U$ and $^{234}U/^{238}U$ activity ratios (or using third-party software such as Iolite for such purpose), we used the MC-ICP-

Table 1: Details of the fossil specimens dated by different methods.

Tabla 1: Detalles de los especímenes fósiles fechados por diferentes métodos.

Lab ID	Excavation number	Description	Purpose
#546	RV001	Caprinae upper molar	Radiocarbon, solution U-series & ESR
#547	RV048	Caprinae lower molar	Laser Ablation U-series
#548	RV051	Caprinae lower molar	Laser Ablation U-series
#549	RV049	Caprinae lower molar	Radiocarbon

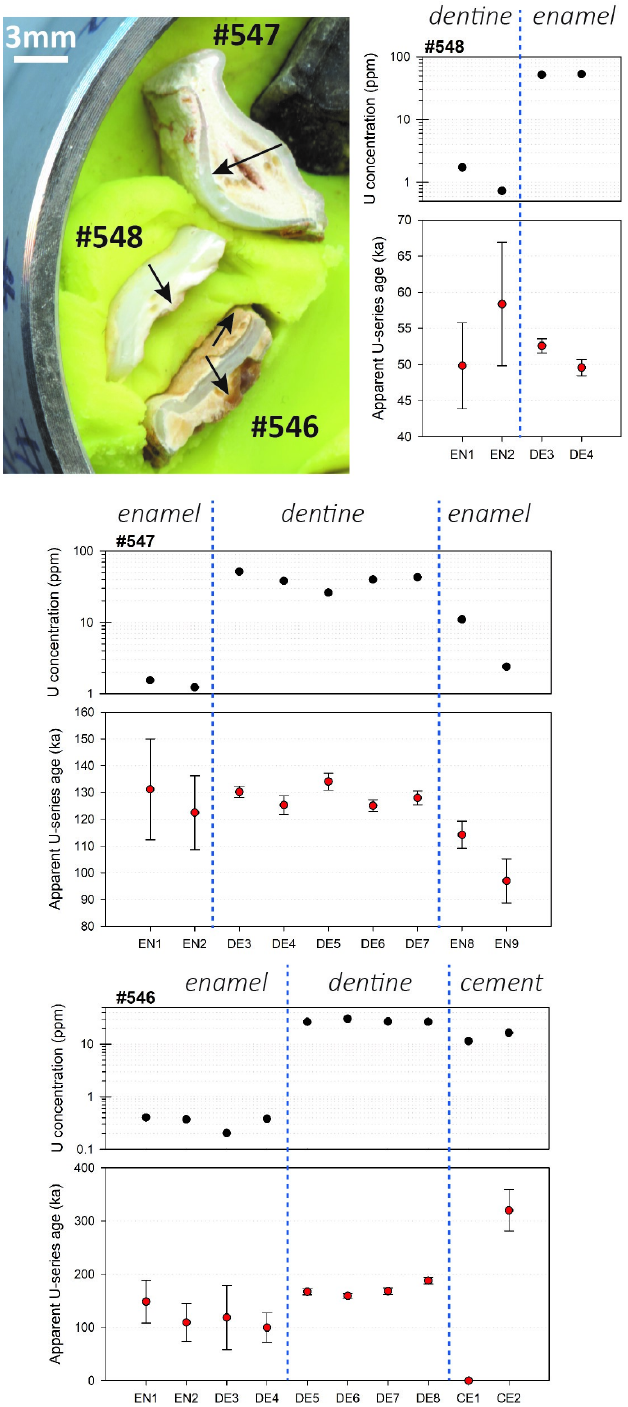

Figure 8: LA-MC-ICPMS U-series analyses performed across tooth fragments from samples #546, #547, and #548. The black arrows indicate the direction of the LA analyses. Numerical data may be found in Table 2. Key: LA= laser ablation; EN= enamel; DE = dentine; CE = cement

Figura 8: Análisis U-Th por MC-ICPMS con ablación laser realizados en secciones transversales de los dientes #546, #547 y #548. Las flechas negras indican la dirección de los análisis por ablación laser. Los datos numéricos se pueden encontrar en la Tabla 2. Leyenda: LA= ablación láser; ES= esmalte; DE = dentina; CE = cemento.

MS online data acquisition software designed for solution analysis to generate baseline fully corrected isotope ratio data directly from the mass spectrometer. Then the $^{230}Th/^{238}U$ activity ratios of the samples were normalized to a homogeneous tooth standard (used in Grün *et al*., 2014) by interpolating through the results of the standard that was repeatedly measured at the beginning and then after every five unknown samples. The $^{230}Th/^{238}U$ activity ratio of this standard has been precisely calibrated by isotope dilution. In each sample, LA transects made of a succession of several rasters were performed across the various dental tissues along the tooth cross-sections (Fig. 8). The resulting mean analytical data obtained for each laser ablation short transect are given in Table 2 and are graphically displayed in Figure 8. This protocol is somehow analogous to micro-drilling of a series of spots along a tooth cross-section for solution MC-ICP-MS dating reported in previous publications (e.g., Price *et al*., 2013, 2017). The difference is that the laser-ablation protocol does not involve any chemical separation of U and Th.

U-series analyses of dental tissues by solution MC-ICPMS: Additional solution U-series analyses were performed on the powdered enamel and dentine from #546 (the sample dated by ESR), following chemical treatment procedures and MC-ICP-MS analytical protocols described elsewhere (e.g., Clark *et al*., 2014; Zhao *et al*., 2009). Powdered sub-samples weighing ~10 mg were spiked with a mixed ^{229}Th-^{233}U tracer and then completely dissolved in concentrated HNO_3. After digestion, each sample was treated with H_2O_2 to decompose trace amounts of organic matter and to facilitate complete sample-tracer homogenization. U and Th were separated using conventional anion-exchange column chemistry using Bio-Rad AG 1-X8 resin. After stripping off the matrix from the column using double-distilled 7N HNO_3 as eluent, 3 ml of a 2% HNO3 solution mixed with a trace amount of HF was used to elute both U and Th into a 3.5-ml pre-cleaned test tube. After column chemistry, the U-Th mixed solution was injected into the MC-ICP-MS through a DSN-100 desolvation nebulizer system with an uptake rate of around 0.07 ml per minute. U-Th isotopic ratio measurement was performed on the MC-ICP-MS using a detector configuration to allow simultaneous measurements of both U and Th. Closed-system U-series ages were calculated using the Isoplot/Ex 3.75 Program (Ludwig, 2003). Results are given in Table 2.

2.4.4. ESR dating

Sample preparation: Tooth #546 was prepared following the same procedure as in Val *et al*. (2021): the enamel layer was mechanically separated from the other dental tissues and both inner and outer surfaces were removed with a dentist drill to eliminate the volume that received an external alpha dose. The dentine attached to the enamel layer was kept aside for subsequent solution bulk U-series analyses (section 2.4.3.). Enamel and dentine were ground and sieved <200 µm.

ESR dose evaluation: Dose evaluation utilized the multiple aliquot additive dose (MAAD) method. The enamel powder of sample #546 was split into eleven aliquots and gamma irradiated at CENIEH (Spain) with a Gammacell 1000 Cs-137 gamma source (dose rate = 6.27 ± 0.14 Gy/min) to the following doses: 0.0, 49.0, 98.1, 147.0, 196.0, 294.1, 392.1, 588.0, 784.0, 980.0 and 1960.0 Gy. Room temperature ESR measurements were carried out at CENIEH with an EMXmicro 6/1 Bruker ESR spectrometer coupled to a standard rectangular ER 4102ST cavity. The following procedure was used to minimize the analytical uncertainties: (i) all aliquots of a given sample were carefully weighted into their corresponding tubes and a variation of <1 mg was tolerated between aliquots; (ii) ESR measurements were performed using a Teflon sample tube holder inserted from the bottom of the cavity to ensure that the vertical position of the tubes remains exactly the same for all aliquots. The following acquisition parameters were used: 1-10 scans, 1 mW microwave power, 1024 points resolution, 15 mT sweep width, 100 kHz modulation frequency, 0.1 mT modulation amplitude, 20

Table 2: LA-MC-ICPMS U-series analytical results. All errors are 2-σ. Key: LA= laser ablation; EN= enamel; DE = dentine; CE = cement. n.c = not calculable. These results are graphically displayed in Fig. 8.

Tabla 2: Resultados analíticos U-Th por LA-MC-ICPMS. Todos los errores son 2-σ. Leyenda: LA= ablación láser; ES= esmalte; DE = dentina; CE = cemento. n.c = no calculable. Estos resultados se muestran gráficamente en la Fig. 8.

Sample	Tissue and LA raster	U (ppm)	$^{230}Th/^{238}U$	$^{234}U/^{238}U$	^{230}Th Age (ka)	Initial $^{234}U/^{238}U$
#547	EN1	1.5	1.177 ± 0.093	1.584 ± 0.035	131.2 ± 18.8	1.85 ± 0.06
#547	EN2	1.2	1.118 ± 0.058	1.568 ± 0.063	122.5 ± 13.8	1.80 ± 0.07
Average ± 2 s.d.					*126.8 ± 12.3*	*1.82 ± 0.06*
#547	DE3	51.6	1.168 ± 0.018	1.580 ± 0.010	130.2 ± 2.2	1.84 ± 0.01
#547	DE4	38.2	1.141 ± 0.023	1.578 ± 0.010	125.3 ± 3.5	1.82 ± 0.01
#547	DE5	26.1	1.179 ± 0.021	1.569 ± 0.011	134.1 ± 3.1	1.83 ± 0.01
#547	DE6	39.9	1.140 ± 0.019	1.577 ± 0.009	125.1 ± 2.2	1.82 ± 0.01
#547	DE7	43.0	1.156 ± 0.019	1.578 ± 0.011	128.0 ± 2.6	1.83 ± 0.01
Average ± 2 s.d.					*128.6 ± 7.5*	*1.83 ± 0.01*
#547	EN8	11.0	1.083 ± 0.030	1.582 ± 0.020	114.2 ± 5.1	1.80 ± 0.02
#547	EN9	2.4	1.021 ± 0.52	1.651 ± 0.045	97.0 ± 8.3	1.86 ± 0.05
Average ± 2 s.d.					*105.6 ± 24.3*	*1.83 ± 0.07*
#548	EN1	1.7	0.558 ± 0.052	1.487 ± 0.042	49.8 ± 6.0	1.56 ± 0.05
#548	EN2	0.7	0.630 ± 0.069	1.482 ± 0.051	58.4 ± 8.6	1.57 ± 0.06
Average ± 2 s.d.					*54.1 ± 12.1*	*1.56 ± 0.01*
#548	DE3	51.7	0.552 ± 0.010	1.414 ± 0.011	52.6 ± 1.0	1.48 ± 0.01
#548	DE4	52.9	0.532 ± 0.012	1.426 ± 0.009	49.6 ± 1.1.	1.49 ± 0.01
Average ± 2 s.d.					*51.1 ± 4.3*	*1.49 ± 0.01*
#546	EN1	0.4	1.149 ± 0.143	1.461 ± 0.085	148.3 ± 40.2	1.70 ± 0.12
#546	EN2	0.4	1.036 ± 0.196	1.556 ± 0.099	109.4 ± 35.3	1.76 ± 0.13
#546	EN3	0.2	1.016 ± 0.289	1.461 ± 0.135	118.7 ± 60.3	1.64 ± 0.18
#546	EN4	0.4	0.922 ± 0.151	1.479 ± 0.103	99.4 ± 27.6	1.63 ± 0.12
Average ± 2 s.d.					*119.0 ± 42.2*	*1.68 ± 0.11*
#546	DE5	26.4	1.314 ± 0.023	1.561 ± 0.016	167.3 ± 5.6	1.90 ± 0.02
#546	DE6	30.4	1.273 ± 0.022	1.550 ± 0.014	159.2 ± 4.5	1.86 ± 0.01
#546	DE7	26.9	1.307 ± 0.027	1.549 ± 0.012	168.2 ± 6.2	1.88 ± 0.02
#546	DE8	26.5	1.397 ± 0.026	1.572 ± 0.012	187.8 ± 6.4	1.97 ± 0.02
Average ± 2 s.d.					*170.6 ± 24.3*	*1.90 ± 0.10*
#546	CE1	11.5	1.901 ± 0.047	1.596 ± 0.019	n.c.	n.c.
#546	CE2	16.5	1.701 ± 0.050	1.601 ± 0.014	319.8 ± 38.9	2.48 ± 0.16

ms conversion time, and 5 ms time constant. All aliquots were successively measured within a short time interval (<1 h). This procedure was repeated two times over successive days without removing the enamel from the ESR tubes between measurements to evaluate measurement and equivalent dose (D_E) precisions (Table 3). The ESR intensities were extracted from the T1-B2 peak-to-peak amplitudes of the ESR signal (Grün, 2000b), and then normalized to the corresponding number of scans and aliquot mass. D_E values were obtained by fitting

a single saturating exponential (SSE) through the mean ESR intensities derived from the repeated measurements. Fitting was performed with Microcal OriginPro 9.1 software, which is based on a Levenberg-Marquardt algorithm by chi-square minimization. Data were weighted by the inverse of the squared ESR intensity ($1/I^2$) and the inverse of the squared experimental errors ($1/s^2$) (Grün & Brumby, 1994). The ESR dose-response curve (DRC) is shown in Figure 9, while numerical fitting results are given in Table 3. The final 1-σ D_E error used for age calculation (Table 4) includes both the fitting and gamma source dose rate errors.

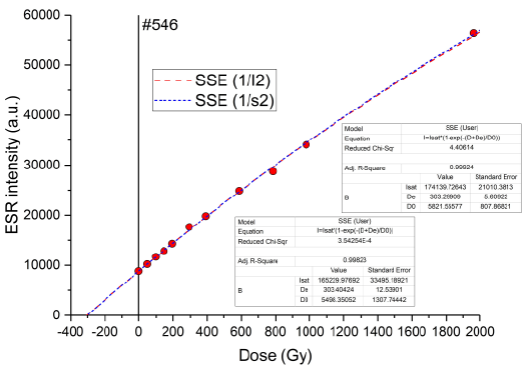

Figure 9: ESR dose-response curve derived from the measurement of enamel sample #546. The ESR intensities and associated errors of each aliquot correspond to the mean value and one standard deviation derived from the repeated ESR measurements. Numerical fitting results may be found in Table 3.

Figura 9: Curvas de crecimiento ESR de la muestra de esmalte #546. Las intensidades ESR y los errores asociados para cada alícuota corresponden al valor medio y una desviación estándar derivada de las mediciones ESR repetidas. Los resultados numéricos se pueden encontrar en la Tabla 3.

Dose rate evaluation and age calculations: No *in situ* evaluation of the gamma dose rate associated with the teeth was performed. Both the beta and gamma dose rates were derived from the laboratory analysis of a sediment sample collected directly from tooth #546. Inductively Coupled Plasma Mass Spectrometry (ICP-MS) analyses were performed on all sediment samples by Genalysis Laboratory Services, following a four-acid digest preparation

Table 3: Detailed ESR results obtained for the enamel of sample #546. Measurement precision is expressed as the mean coefficient of variation obtained for all the aliquots of a given sample after the two or three repeated measurements. DE precision is the variation of the DE values derived from the repeated measurements of a given sample.

Tabla 3: Resultados detallados de ESR obtenidos para el esmalte de la muestra #546. La precisión de la medida se expresa como el coeficiente medio de variación obtenido para todas las alícuotas de una muestra dada después de dos o tres medidas repetidas. La precisión DE es la variación de los valores DE derivados de las mediciones repetidas de una muestra dada.

Sample	**#546**
Average weight per aliquot (mg)	14.9 ± 0.3
Number of repeated measurements	2
Measurement precision (%)	0.8
SSE fitting (data weighting by $1/I^2$)	
D_E precision (%)	1.8
Adj. r-Square	0.998
D_{E1} (Gy)	303 ± 13
D_{max} (Gy)	1960
D_{max}/D_E	6.5
SSE fitting (data weighting by $1/s^2$)	
Adj. r-Square	0.999
D_{E2} (Gy)	303 ± 6
D_{max} (Gy)	1960
D_{max}/D_E	6.5

procedure. The following parameters were used for the dose rate calculations: an alpha efficiency of 0.13 ± 0.02 (Grün & Katzenberger-Apel, 1994), Monte-Carlo beta attenuation factors from (Marsh, 1999), dose-rate conversion factors from (Guérin *et al*., 2011). Water content values (% wet weight) were assumed to be 5 ± 3 wt.% and 15 ± 5 wt.% in dentine and sediment, respectively. A long-term depth value of 1 ± 1 m was considered for the cosmic dose rate evaluation. Post-Rn equilibrium was assumed in dental tissues and sediment. Beta dose rate evaluation was performed using a sample geometry sediment/enamel/dentine. DATA (Grün, 2009), a Quick Basic-based program was used to calculate US-ESR based on the US model defined

Table 4: Data inputs and outputs associated with the ESR age calculations. All errors are given at a 1-σ confidence level.

Tabla 4: Datos asociadas con los cálculos de edad ESR. Todos los errores se dan con un nivel de confianza de 1-σ.

Sample	**#546**
Enamel	
Dose (Gy)	303 ± 9
U (ppm)	0.390 ± 0.000
$^{234}U/^{238}U$	1.489 ± 0.002
$^{230}Th/^{234}U$	0.507 ± 0.001
$^{230}Th/^{232}Th$	860
Apparent U-series age (ka)	73.6 ± 0.3
Initial$^{234}U/^{238}U$	1.602 ± 0.002
Alpha Efficiency	0.13 ± 0.02
Water content (%)	0
Initial enamel thickness (µm)	613 ± 61
Dentine	
U (ppm)	19.25 ± 0.02
$^{234}U/^{238}U$	1.551 ± 0.001
$^{230}Th/^{234}U$	0.763 ± 0.001
$^{230}Th/^{232}Th$	1666
Apparent U-series age (ka)	138.3 ± 0.7
Initial$^{234}U/^{238}U$	1.815 ± 0.002
Water (%)	5 ± 3
Removed enamel thickness (µm)	62 ± 6
Sediment	
U (ppm)	0.82 ± 0.07
Th (ppm)	3.08 ± 0.14
K (%)	0.48 ± 0.02
Water (%)	15 ± 5
Removed thickness (µm)	47 ± 5
US-ESR age calculations	
Internal dose rate (µGy/a)	37 ± 6
Beta dose rate, dentine (µGy/a)	268 ± 30
Beta doserate, sediment (µGy/a)	90 ± 9
Gamma dose rate (µGy/a)	297 ± 21
Cosmic dose rate (µGy/a)	183 ± 18
Total dose rate (µGy/a)	875 ± 44
p enamel	1.62
p dentine	-0.20
US-ESR age (ka)	**346 +23 -21**
EU-ESR (ka)	**253 ± 12**
CSUS-ESR (ka)	**418 ± 28**

by Grün *et al*. (1988) and CSUS-ESR age estimates. The CS model defined by Grün (2000a) is based on the assumption of a closed system behavior after a rapid uranium uptake event in dental tissues. The CSUS-ESR age is usually considered as providing a maximum age constraint for the fossil. US and CSUS models are typically considered to encompass all possible uptake scenarios. Early uptake (EU)-ESR ages were also calculated for comparison. All US-ESR data inputs and outputs are given in Table 4. More information about the combined U-series/ESR dating method may be found in Duval (2015).

3. Results and Discussion

3.1. Paleontological and taxonomic analysis

Our analysis shows that 45 remains are post-cranial elements, including mostly elements from the appendicular skeleton (N=33), while 1 cranial bone and 11 teeth may also be identified (Figs. 4-7; see detailed information in Table 5).

Regarding the taxonomic assessment, the anatomical characters are not sufficiently preserved to enable an attribution to the genus or species level. We nevertheless identified that the assemblage is largely dominated by the presence of remains attributed to the subfamily Caprinae (~67%): 34 remains may be securely attributed to this subfamily, while 4 additional specimens may share a similar attribution. In the sample, one single specimen of the Cervidae family is also represented. The fossil assemblage includes 4 specimens that belong to Carnivores, but only 1 of these can be attributed to a subfamily (the Felinae subfamily). Finally, one remain belongs to the Order Lagomorpha, and 13 cannot be taxonomically determined (indet.). Among these skeletal remains, 35 are assessed as adult/mature remains, 7 as immature remains, and 15 as indet. The most repeated Caprinae remain is the left tibia (N=5, 4 mature, and 1 immature), resulting in the calculation of a

Table 5: Basic description of the fossil remains collected from Los Villares locality. Key: N/A = not applicable; Indet. = Indeterminate; * = possible attribution, to be confirmed in the future.

*Tabla 5: Descripción básica de los restos fósiles recolectados en la localidad de Los Villares. Clave: N/A = no aplicable; indet. = Indeterminado; * = posible atribución, por confirmar en el futuro.*

	Anatomy	Part	Laterality	Taxa	Development
RV001	Teeth	Partial	Indet.	Caprinae	Adult
RV003	Teeth	Proximal	Left	Caprinae	Adult
RV004	Teeth	Partial	Indet.	Caprinae	Adult
RV032	Teeth	Partial	Indet.	Caprinae	Adult
RV044	Teeth	Distal	Left	Caprinae	Adult
RV046	Teeth	Distal	Left	Caprinae	Adult
RV047	Teeth	Complete	Left	Caprinae	Adult
RV048	Teeth	Complete	Indet.	Caprinae	Adult
RV049	Teeth	Proximal	Indet.	Caprinae	Adult
RV050	Teeth	Proximal	Left	Caprinae	Adult
RV051	Teeth	Complete	Indet.	Caprinae	Adult
RV007	Calcaneus	Complete	Indet.	Caprinae	Adult
RV022	Calcaneus	Body	N/A	Caprinae	Immature
RV029	Calcaneus	Distal	Left	Caprinae	Adult
RV017	Scapula	Diaphysis	Indet.	Caprinae	Adult
RV011	Phalanx	Shaft	Indet.	Caprinae	Adult
RV012	Phalanx	Proximal	Right	Caprinae	Adult
RV005	Femur	Proximal	Right	Caprinae	Adult
RV006	Femur	Proximal	Left	Caprinae	Immature
RV002	Humerus	Distal	Left	Caprinae	Adult
RV031	Humerus	Distal	Left	Caprinae	Immature
RV038	Humerus	Distal	Right	Caprinae	Adult
RV009	Metacarpal	Indet	N/A	Caprinae	Adult
RV055	Phalanx	Indet.	Left	Caprinae	Adult
RV010	Tibia	Proximal	Left	Caprinae	Adult
RV021	Tibia	Indet.	N/A	Caprinae	Adult
RV025	Tibia	Distal	Left	Caprinae	Adult
RV030	Tibia	Diaphysis	Indet.	Caprinae	Immature
RV053	Tibia	Distal	Left	Caprinae	Adult
RV014	Ulna	Distal	Left	Caprinae	Immature
RV018	Ulna	Proximal	Left	Caprinae	Immature
RV020	Ulna	Partial	Indet.	Caprinae	Adult
RV013	Vertebra	Indet.	Indet.	Caprinae	Immature
RV041	Metacarpal	Indet.	Indet.	Caprinae	Indet.
RV019	Scapula	Indet.	Indet.	Caprinae*	Adult
RV008	Phalanx	Indet.	Indet.	Caprinae*	Adult
RV037	Femur	Distal	Left	Caprinae*	Indet.
RV027	Calcaneus	Distal	Left	Caprinae*	Adult

RV056	Teeth	Indet.	Indet.	Carnivore*	Adult
RV043	Tibia	Indet.	Indet.	Cervidae	Adult
RV054	Mandible	Proximal	Right	Felinae	Adult
RV016	Rib	Indet.	Indet.	Indet.	Indet.
RV024	Coxal bone	Distal	Right	Indet.	Indet.
RV042	Scapula	Partial	Indet.	Indet.	Indet.
RV033	Indet.	Proximal	Right	Indet.	Indet.
RV034	Indet.	Partial	Indet.	Indet.	Indet.
RV035	Indet.	Partial	Indet.	Indet.	Indet.
RV036	Indet.	Partial	Indet.	Indet.	Indet.
RV039	Indet.	Partial	Indet.	Indet.	Indet.
RV040	Indet.	Partial	Indet.	Indet.	Indet.
RV028	Tibia	Partial	Indet.	Indet.	Indet.
RV023	Vertebra	Proximal	Indet.	Indet.	Indet.
RV026	Vertebra	Complete	Left	Indet.	Indet.
RV045	Femur	Hemimandible	Indet.	Indet.	Adult
RV052	Femur	Complete	Indet.	Lagomorpha	Adult
RV015	Long bone	Partial	Indet.	Large Carnivore Indet.	Indet.
RV057	Metacarpal	Various	Indet.	Small Carnivore Indet.	Adult

minimum number of 5 Caprinae individuals. Additionally, 1 Felinae, 1 Cervidae, and 1 Lagomorpha were also assessed, totaling a minimum number of 8 individuals and 4 taxa in the assemblage.

3.2. Preliminary taphonomic study

So far, the fossil record recovered at the Los Villares site is scarce. However, we were still able to analyze the fracture pattern in 10 long bones found at the site. The analysis of the fracture outlines shows that most of the bones have irregular edges. The relation between the shaft length and preserved length shows that no bones preserve more than half of their length. Our study indicates that the long bones were fractured when they were already dry, and overall show no evidence of human activity.

The only exception is the remain RV-017, which does show potential evidence of human-made alterations (i.e., cut mark; Fig. 10). This possibility was statistically evaluated through an artificial intelligence (AI) approach. Results show that all the AI models consistently agree in classifying this bone surface modification (BSM) as a cut mark (Table 6). Moreover, four out of the five models

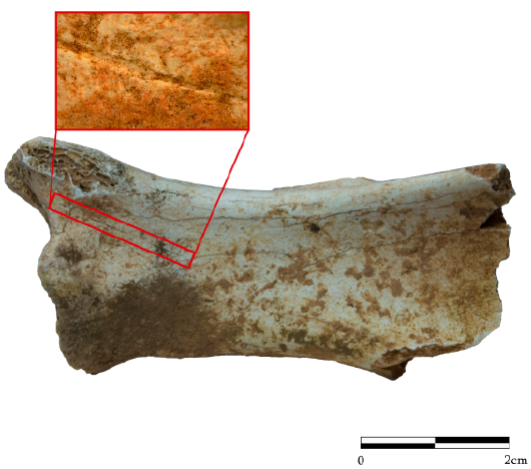

Figure 10: Detailed picture of the potential human-made cut mark found on fossil RV-017.

Figura 10: Imagen detallada de la posible marca de corte hecha por humanos encontrada en el fósil RV-017.

Table 6: Classification values for the bone surface modifications (BSM) image analyzed. The table shows the confidence of each model architecture when classifying the BSM into the different three classes. The categories definition can be found in Domínguez-Rodrigo *et al*. 2020.

Tabla 6: Valores de clasificación para la imagen de modificaciones de la superficie ósea (BSM) analizada. La tabla muestra la confianza de cada modelo de arquitectura al clasificar el BSM en las tres clases diferentes. La definición de las categorías se encuentra en Domínguez-Rodrigo et al. 2020.

	Tooth mark	Cut mark	Trampling mark
DenseNet201	21.79%	77.20%	0.99%
VGG16	0%	100%	0%
VGG19	0.04%	99.95%	0.01%
InceptionV3	0.20%	99.78%	$3.21 \cdot 10^{-5}$%
ResNet50	0.73%	99.25%	$1.79 \cdot 10^{-5}$%

achieve confidence rates of 99% or higher, strengthening the reliability of this identification. Also, both parallel and sequential model architectures achieve similar results, showing that they are equally suitable for these classification problems and thus, both should be considered when conducting AI analyses.

3.3. Geochemical characterization of the breccia

Grain size analysis shows that the sediment is silty sand, almost equally dominated by the sandy (44.1 %) and silty (41.5%) fractions, while clay represents about 14.4 % of the total (Table 7). Quantitative XRF analysis shows that it is largely dominated by Ca (45.4%) and Si (11.01 %), most likely resulting from carbonates and silicates, respectively (Table 8). The non-negligible amount of Al (4.0%) may illustrate the presence of clays, in agreement with grain size analysis, and the presence of feldspars.

Table 7: XRF results from the brecciated sediment showing the relative proportions of various major elements in their oxidized state. LOI = loss of ignition.

Tabla 7: Resultados XRF del sedimento brechificado que muestran las proporciones relativas de varios elementos principales en su estado oxidado. LOI = loss of ignition.

	Amount (%)
SiO_2	11.05
Al_2O_3	4.04
Fe_2O_3	1.78
MnO	0.027
MgO	0.39
CaO	45.39
Na_2O	0.03
K_2O	0.58
TiO_2	0.21
P_2O5	1.25
SO_3	0.02
LOI	35.24

3.4. Dating results

3.4.1. Radiocarbon dating

Although theoretically bone with 0.2 %N should contain the ≥ 1 % collagen required for radiocarbon dating, (Brock *et al*., 2012) found bone containing ≥ 0.7 % N had a 73 % chance of containing sufficient collagen when extracted and cleaned with an ultrafiltration protocol. Unfortunately, samples from Los Villares contained between 0.02-0.07 %N and were not datable with radiocarbon.

3.4.2. LA U-series analyses

High-resolution LA U-series analyses were performed to (i) evaluate the spatial distribution of U-series data across dental tissues of samples #546, #547, and #547, and (ii) evaluate the suitability of sample #546 for combined U-series/ESR dating.

Table 8: Granulometric results obtained from the brecciated sediment using the Robinson pipette method.

Tabla 8: Resultados granulométricos obtenidos del sedimento brechificado utilizando el método de la pipeta de Robinson.

Size class	Fraction (µm)	retained (% weight)
Sand	2000-500	30.3
	500-212	6.6
	212-53	7.2
	Total sand	44.1
Silt	53-20	13.0
	20-2	28.5
	Total silt	41.5
Clay	<2	14.4

Sample #547 shows apparent ages that are systematically >100 ka across dentine and enamel: the first enamel domain (EN1-EN2) analyzed, and the dentine return overall consistent ages of ~127 ka and ~129 ka, respectively, while the second enamel domain yields younger estimates of ~106 ka. The asymmetric shape of the age profile suggests that there is a more recent uranium uptake overprint from one side of the tooth.

In comparison, sample #548 shows much younger age estimates, although overall consistent across dentine (~51 ka) and enamel (~54 ka) (Table 3).

Finally, LA analysis of sample #546 returns somewhat consistent U-series data within enamel and dentine domains. No recent overprint is observed within the tooth. The uranium concentration varies between 0.2 and 0.4 ppm in enamel, and between 26 and 30 ppm in dentine. Similarly, the apparent U-series ages vary within a relatively narrow range (dentine) or are all 1-σ consistent (enamel). Pseudo bulk mean values of ~119 ka and ~171 ka are obtained for the enamel and dentine, respectively. In contrast, the cement returns more scattered U-series data, with apparent U-series age estimates that are close or even beyond secular equilibrium, indicating that the tissue is experiencing uranium leaching. While the LA raster CE2 provides an apparent age result of 319.8 ± 38.9 ka (Table 3) that could be interpreted as a minimum age constraint for the fossil, the occurrence of uranium leaching in this tissue (LA raster CE1) suggests that the reliability of this result should be considered with caution.

All apparent U-series age estimates should be regarded as minimum age constraints (provided there is no evidence for uranium leaching), since uranium uptake may sometimes be significantly delayed after the death of the organism. Consequently, a minimum age of ~130 ka, ~50 ka, and ~170 ka may be proposed for samples #547, #548, and #546, respectively. Additionally, these results indicate that the age of the fossil specimens lies beyond the Radiocarbon time range.

Finally, U-series data collected for sample #546 show that (i) the enamel tissue has very low uranium concentrations (<0.5 ppm), and (ii) there is no evidence of uranium leaching in dentine and enamel tissues (i.e., finite age can be calculated), unlike in cement. These two observations indicate that the tooth is overall suitable for ESR dating: sample preparation for ESR dating was therefore focused on an area of the tooth without cement.

3.4.3. ESR dose evaluation

Measurement precision achieved is overall excellent (0.8%), resulting in a D_E repeatability of < 2 % (Table 3). D_E value obtained over the full irradiation dose range is 303 ± 13 Grays (Gy) (Fig. 9). Goodness-of-fit is excellent (adjusted $r^2 > 0.99$). The corresponding D_{max}/D_E ratio value falls within the recommended range by Duval and Grün (2016) for a D_E value of this magnitude ($5 < D_{max}/D_E < 10$). Additional dose-response curve (DRC) fitting was performed using data weighting by $1/s^2$, yielding virtually the same D_E value (Table 3). This illustrates the negligible impact of data weighting on the fitting outcome.

3.4.4. Combined U-series and ESR age calculations

Solution U-series analyses of the bulk powdered dental tissues return apparent age estimates of ~74 and ~138 ka (Table 4). As minimum age constraints for the fossil, they are not incompatible with the LA results, which are somewhat older for both tissues. The differences observed between solution and LA analyses most likely result from the spatial heterogeneity of U-series data within the tooth, which may sometimes be significant since the samples were collected from different parts of the tooth. Combined U-series/ESR age calculations were performed using solution U-series analytical results since the powdered enamel sample is the same that was independently analyzed by ESR, while the dentine sample was directly attached to this enamel sample.

Age calculation based on the US model (Grün *et al*., 1988) yields a combined US-ESR estimate of 346 +23 -21 ka for tooth #546 (Table 4). Modeled p-values indicate a recent uptake in the enamel (>0), and a somewhat early uptake in the dentine instead (p< 0). Dose rate evaluation indicates that the beta component from the dentine and the gamma component represents about 30% of the total value. The cosmic dose rate is also not negligible, representing about 20 % of the total value.

Three main sources of uncertainty may be identified. First, the absence of *in situ* dosimetry precludes a proper evaluation of the true gamma dose rate. Given the non-negligible weight of this component in the dose rate evaluation, we anticipate that any heterogeneity from the surrounding sedimentary environment, may potentially significantly impact the calculated age result. However, this is presently impossible to quantify. In contrast, the influence of both long-term depth and long-term water content can be roughly assessed. Age simulations using depth values of 0.5, 2 and 5 m return US-ESR estimates of ~338 ka, ~358 ka, and ~386 ka, respectively, i.e., -2%, +3%, and +12 % compared to the value initially calculated. In all cases, the calculated values remain 1-σ consistent with the age of 346 +23 -21 ka. Variation of the long-term water content by ± 5% and ± 10% compared with the initial value, return US-ESR estimates that vary by ± 3-4% and ± 7-8%, respectively. Again, all the calculated ages remain 1-σ consistent with the age initially calculated. In summary, even when using somewhat extreme long-term depth and water content values, the US-ESR age remains between 300 and 400 ka. This chronology would position the fossil assemblage between MIS 9 and 11 (Lisiecki & Raymo, 2005).

3.5. Significance of Los Villares fossil assemblage in the Southern Plateau and the Spanish archeo-paleontological record

To the best of our knowledge, this is the first directly dated fossil assemblage of the Middle Pleistocene age reported in the Guadiana Basin (Southern Plateau), filling a gap in the Pleistocene fossil record of the Iberian Peninsula (Fig. 11). In the Northern Plateau, the Atapuerca Complex (Burgos) includes Galería TG8 level dating >350 ka (Demuro *et al*., 2014; Pérez-González *et al*., 2001), Sima de los Huesos dated to around 450 ka (Arsuaga *et al*., 2014) and the Gran Dolina TD10 level with an age of between 320-370 ka (Falguères *et al*., 1999; Moreno *et al*., 2012). In the surroundings of the Iberian chain, there are Middle Pleistocene fossil sites linked to river terraces such as Torralba and Ambrona complex (Soria, Castilla y León) and Cuesta de la Bajada (Teruel), at ages of 314-366 ka for AS6 from the Lower Complex of Ambrona (AS1 to AS6; Falguères *et al*., 2006)), and 243-337 ka (for Cuesta de la Bajada; Santonja *et al*., 2014).

In the upper Tagus Basin, Áridos 1 and 2 have yielded micro- and large mammals as well as Acheulean lithic artifacts (Santonja *et al*., 2001 and references therein). They belong to the stratigraphic unit Arganda I, which has been chronologically constrained to between 295 and 365 ka based on ESR and Amino Acid Racemization methods (Panera *et al*., 2011).

Downstream in the Tagus Basin, the Gruta da Aroeira (Portugal) contains Mousterian levels that include a partial human skull and have been dated to 390-436 ka (Daura *et al*., 2017). In the Coastal-Catalan Ranges, levels XVII-XV from Cova del Bolomor (Fernández Peris *et al*., 2008), have been dated around 347-242 ka. Finally, in the South of the Iberian Peninsula, the Acheulean assemblage and associated fauna excavated from the site of Solana del Zamborino (Guadix-Baza basin) have been recently chronologically constrained to between around 300-480 ka using magnetostratigraphy (Álvarez-Posada *et al*., 2017).

Moreover, from an archeological perspective, the identification of a cut mark on one of the fossils suggests a human presence in the area around 300-400 ka. The chronology of the Los Villares site falls within a period of special interest, in which several Spanish localities have provided very distinct lithic assemblages attributed to either Acheulean or Middle Paleolithic technocomplexes. For some authors, this suggests that different human groups might have been coexisting in the Iberian Peninsula during the Middle Pleistocene (e.g., Méndez-Quintas *et al*., 2018; Santonja *et al*., 2014). For example, Cuesta de la Bajada (Teruel) site has yielded a Middle Paleolithic lithic industry and associated fauna possibly correlated to the MIS 9, while the Ambrona archaeo-paleontological site, located on the NE edge of the Central System has produced an Acheulean assemblage of somewhat close chronology (e.g., Duval, 2018; Falguères *et al*., 2006).

Among the archeological sites in the region of Los Villares, the Upper Guadiana Basin, it is worth highlighting El Sotillo (Arroyo & de la Torre, 2013; Ciudad Serrano *et al*., 1983), Albalá (Arroyo & de la Torre, 2013; Santonja *et al*., 1977), El Martinete (Querol & Santonja, 1983), Porzuna (Vallespí *et al*., 1979) and Dehesa and Molino del Emperador (López-Recio *et al*., 2001; Morín de Pablos *et al*., 2007). While a large number of Acheulean stone tools have been found in all (e.g., > 1000 bifaces in Porzuna), Molino del Emperador is the only site with a supposedly clear chronostratigraphic context: it is located on the ter-

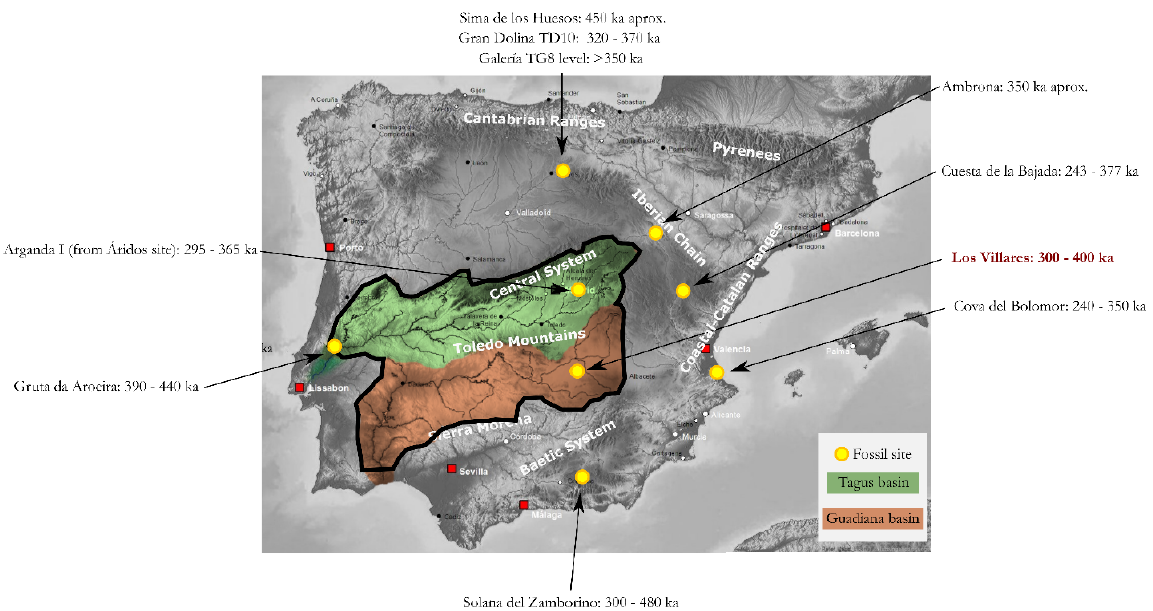

Figure 11: Main Middle Pleistocene localities in the Iberian Peninsula with similar ages to Los Villares locality.

Figura 11: Principales localidades del Pleistoceno Medio en la Península Ibérica con edades similares a la localidad de Los Villares.

race +13/16m of the Guadiana River, which has been dated by OSL to around 150 ka (López-Recio *et al*., 2004). However, this age should be treated with caution, given some methodological issues recently reported by Garcia-Vadillo *et al*. (2021). The chronologies of all other sites are based on the typological assignment of the lithic assemblages and are therefore more difficult to securely place in time (Fernández *et al*., 2005).

4. Conclusions

The results from this multidisciplinary study show the Los Villares fossil site is likely to be a significant archeo-palaeontological archive in the Southern Iberian Plateau. Not only does it have a high density of well-preserved skeletal and dental remains, but it also has a crucial chronology and may contain evidence of human activity. As such, it will fill a gap of knowledge in an area characterized by a very limited Pleistocene fossil and archeological record compared to other Iberian regions (García-Martínez, 2019). Our multi-technique dating approach provides the first direct age constraints for the archeo-paleontological assemblage, positioning Villares around MIS 9-11 i.e., within a time range of great interest for the understanding of human migrations and occupations in the Iberian Peninsula during the Middle Pleistocene.

However, we would also like to clearly acknowledge the existing limitations of the present work to avoid any overinterpretation of these promising results. For example, the ESR chronology is based on a very limited number of samples analyzed, and there is inherent uncertainty associated with the gamma dose rate reconstruction and the evaluation of long-term depth and water content. Nevertheless, considering most sources of uncertainty, our simulations suggest that the age of the fossil specimen remains systematically between 300 and 400 ka. In addition, the presence of a cut mark suggests possible human activity at the site, although other hypotheses such as carnivore origin cannot be ruled out until new additionnal evidence of human presence can be provided.

Based on these first results, there is now a crucial need to collect further data about the spatial and stratigraphic extension of the fossil assemblage through a proper systematic excavation campaign. In particular, future investigations will focus on the detailed description of the stratigraphic and geological context. This will enable us to determine whether the fossil assemblage represents a single depositional event.

Acknowledgments

We thank José Ramos Sanz, president of Los Villares house state (Ruidera, Ciudad Real), and Antonio Ruiz Reinosa, guard of the house state, for their kindness and collaboration regarding the preservation of the archaeo-paleontological heritage in Los Villares. We also thank Dr. Carlos Arroyo and Dr. Javier Campos Fernández de Sevilla for the news about the findings. We are grateful to Salvador Jiménez and Dr. Santiago Domínguez for their initial input on the paleontology, archeology, and geology of the area. María Jesús Alonso Escarza, Leticia Miguens Rodríguez and Javier Iglesias Cibanal (CENIEH), and Faye Liu (UQ) provided invaluable support for the ESR and U-series dating analyses. Aspects of the dating analyses have been funded by the Spanish Ramón y Cajal Fellowship RYC2018-025221-I granted to MD. U-series dating analyses were carried out within the framework of the existing Brisbane Geochronology Alliance between Griffith University, the University of Queensland, and the Queensland University of Technology. The "Juan de la Cierva Formación" program (FJCI-2017-32157), from the Spanish Ministry of Science and Innovation, funds DGM. Grain size and XRF analyses were both performed at CENIEH by Leticia Miguens Rodríguez and Javier Iglesias Cibanal (Technical report I-2020-009-GE), and by Ana Alvaro Gallo (Technical report AM I-2020-016), respectively.

References

Abellán, N., Jiménez-García, B., Aznarte, J., Baquedano, E., & Domínguez-Rodrigo, M. (2021). Deep learning classification of tooth scores made by different carnivores: achieving high accuracy when comparing African carnivore taxa and testing the hominin shift in the balance of power. *Archaeological and Anthropological Sciences*, *13*(2), 1-14. https://doi.org/10.1007/s12520-021-01273-9

Aguirre, E. (1989). Vertebrados del Pleistoceno continental. *Mapa Del Cuaternario de España, Escala 1: 1.000 000*, 47-69.

Alberdi, M. T., Jiménez, E., Mazo, A. V., Morales, J., Sesé, C., & Soria, D. (1984). Paleontología y biostratigrafía de los yacimientos villafranquienses de Las Higueruelas y Valverde de Calatrava II (Campo de Calatrava, Ciudad Real). *Actas I Reunión de Estudios Regionales de Castilla-La Mancha*, *3*, 255-277.

Álvarez, M., Cirujano, S., Montero González, E., Roja, C., Rodrigo, M., Piña, E., Rodríguez, J. C., Soriano, Ó., Aboal, M., & Marín, J. P. (2007). Ecología acuática y sociedad de las lagunas de Ruidera. *CSIC, Madrid*.

Álvarez-Posada, C., Parés, J. M., Sala, R., Viseras, C., & Pla-Pueyo, S. (2017). New magnetostratigraphic evidence for the age of Acheulean tools at the archaeo-paleontological site "Solana del Zamborino" (Guadix-Baza Basin, S Spain). *Scientific Reports*, *7*(1), 1-9. https://doi.org/10.1038/s41598-017-14024-5

Arribas Herrera, A., & Palmqvist, P. (1998). Taphonomy and paleoecology of an assemblage of large mammals: hyaenid activity in the lower Pleistocene site at Venta Micena (Orce, Guadix-Baza Basin, Granada, Spain). *Geobios*, *31*, 3-47. https://doi.org/10.1016/S0016-6995(98)80056-9

Arribas Herrera, A., Riquelme, J. A., Palmqvist, P., Garrido, G., Hernández, R., Laplana, C., Soria, J. M., Viseras, C., Durán, J. J., & Gumiel, P. (2001). Un nuevo yacimiento de grandes mamíferos villafranquienses en la Cuenca de Guadix-Baza (Granada): Fonelas P-1, primer registro de una fauna próxima al límite Plio-Pleistoceno en la Península Ibérica. *Boletín Geológico y Minero*, *112*(4), 3-34.

Arribas Herrera, A., & Jordá Pardo, J. F. (1999). Los mamíferos del Cuaternario kárstico de Guadalajara (Castilla-La Mancha, España). In *La Huella del Pasado. Fósiles de Castilla-La Mancha* (pp. 327-353). Array.

Arroyo, A., & de la Torre, I. (2013). Acheulean large flake technology in Campo de Calatrava (Ciudad Real, Spain). *Archaeology, Ethnology, and Anthropology of Eurasia*, *41*(4), 2-10. https://doi.org/10.1016/j.aeae.2014.07.002

Arsuaga, J. L., Carretero, J.-M., Lorenzo, C., Gómez-Olivencia, A., Pablos, A., Rodríguez, L., García-González, R., Bonmatí, A., Quam, R. M., Pantoja-Pérez, A., Martínez, I., Aranburu, A., Gracia-Téllez, A., Poza-Rey, E., Sala, N., García, N., Alcázar de Velasco, A., Cuenca-Bescós, G., Bermúdez de Castro, J. M., & Carbonell, E. (2015). Postcranial morphology of the middle Pleistocene humans from Sima de los Huesos, Spain. *Proceedings of the National Academy of Sciences*, *112*, 11524-11529. http://www.pnas.org/content/early/2015/08/27/1514828112.abstract. https://doi.org/10.1073/pnas.1514828112

Arsuaga, J. L., Lorenzo, C., Carretero, J. M., Gracia, A., Martínez, I., García, N., Bermudez de Castro, J. M., & Carbonell, E. (1999). A complete human pelvis from the middle Pleistocene of Spain. *Nature*, *399*(6733), 255-258. https://doi.org/10.1038/20430

Arsuaga, J. L., Martínez, I., Arnold, L. J., Aranburu, A., Gracia-Téllez, A., Sharp, W. D., Quam, R. M., Falguères, C., Pantoja-Pérez, A., Bischoff, J., Poza-Rey, E., Parés, J. M., Carretero, J. M., Demuro, M., Lorenzo, C., Sala, N., Martinón-Torres, M., García, N., Alcázar de Velasco, A., … Carbonell, E. (2014). Neandertal roots: Cranial and chronological evidence from Sima de los Huesos. *Science*, *344*(6190), 1358-1363. https://doi.org/10.1126/science.1253958

Badiola, E. R., Mazo, A. V., & Ruiz, P. R. (2007). El yacimiento de Las Higueruelas, Alcolea de Calatrava (Ciudad Real): procesos diagenéticos y volcanismo asociado. *Estudios Geológicos*, *63*(2), 67-86. https://doi.org/10.3989/egeol.07632194

Baldeón, A. (1993). El yacimiento de Lezetxiki (Gipuzkoa, País Vasco): los niveles musterienses. *Munibe*, *54*, 3-97.

Baquedano, E., Márquez, B., Pérez-González, A., Mosquera Martínez, M., Huguet Pamiès, R., Espinosa, J. A., Sanchez Romero, L., Panera, J., & Arsuaga, J. L. (2012). Neandertales en el Valle del Lozoya: los yacimientos Paleolíticos del Calvero de la Higuera (Pinilla del Valle, Madrid). *Mainake*, *33*, 83-100.

Barandiarán, I., & Altuna, J. (1973). *La Cueva de Los Casares (Riba de Saelices, Guadalajara). Excavaciones Arqueológicas en España.* (Vol. 76). Ministerio de Educación y Ciencia.

Bermúdez de Castro, J. M., Arsuaga, J. L., Carbonell, E., Rosas, A., Martínez, I., & Mosquera, M. (1997). A Hominid from the Lower Pleistocene of Atapuerca, Spain, Possible Ancestor to Neandertals and Modern Humans. *Science*, *276*, 1392-1395. https://doi.org/10.1126/science.276.5317.1392

Bermúdez de Castro, J. M., Martinón-Torres, M., Gomez-Robles, A., Prado-Simon, L., Martin-Frances, L., Lapresa, M., Olejniczak, A., Carbonell, E., Gracia, A., Olejniczak, A., Prado-Simon, L., Gomez-Robles, A., Lapresa, M., Carbonell, E., Arsuaga, J. L., & Bermudez de Castro, J. M. (2011). Early Pleistocene human mandible from Sima del Elefante (TE) cave site in Sierra de Atapuerca (Spain): a paleopathological study. *J Hum Evol*, *61*(1), 12-25. https://doi.org/10.1016/j.jhevol.2011.01.004

Bermúdez de Castro, J. M., Martinón-Torres, M., Martín-Francés, L., Modesto-Mata, M., Martínez-de-Pinillos, M., García, C., & Carbonell, E. (2017). Homo antecessor: The state of the art eighteen years later. *Quaternary International*, *433*, 22-31. https://doi.org/10.1016/j.quaint.2015.03.049

Blain, H.-A., Santonja, M., Pérez-González, A., Panera, J., & Rubio-Jara, S. (2014). Climate and environments during Marine Isotope Stage 11 in the central Iberian Peninsula: the herpetofaunal assemblage from the Acheulean site of Áridos-1, Madrid. *Quaternary Science Reviews*, *94*, 7-21. https://doi.org/10.1016/j.quascirev.2014.04.009

Brock, F., Wood, R., Higham, T. F. G., Ditchfield, P., Bayliss, A., & Ramsey, C. B. (2012). Reliability of nitrogen content (% N) and carbon: nitrogen atomic ratios (C: N) as indicators of collagen preservation suitable for radiocarbon dating. *Radiocarbon*, *54*(3-4), 879-886. https://doi.org/10.1017/S0033822200047524

Byeon, W., Domínguez-Rodrigo, M., Arampatzis, G., Baquedano, E., Yravedra, J., Maté-González, M. A., & Koumoutsakos, P. (2019). Automated identification and deep classification of cut marks on bones and its paleoanthropological implications. *Journal of Computational Science*, *32*, 36-43. https://doi.org/10.1016/j.jocs.2019.02.005

Carretero, J. M., Arsuaga, J.-L., Martinez, I., Quam, R. M., Lorenzo, C., Gracia, A., & Ortega, A. I. (2004). Los humanos de la Sima de los Huesos (Sierra de Atapuerca) y la evolucion del cuerpo en el género Homo. In E. Baquedano (Ed.), *Homenaje a Emiliano Aguirre* (Vol. 4, pp. 120-136). Museo Arqueologico Regional.

Casas-Sainz, A. M., & de Vicente, G. (2009). On the tectonic origin of Iberian topography. *Tectonophysics*, *474*(1-2), 214-235. https://doi.org/10.1016/j.tecto.2009.01.030

Chetlur, S., Woolley, C., Vandermersch, P., Cohen, J., Tran, J., Catanzaro, B., & Shelhamer, E. (2014). cudnn: Efficient primitives for deep learning. *ArXiv Preprint ArXiv:1410.0759*.

Cifuentes-Alcobendas, G., & Domínguez-Rodrigo, M. (2019). Deep learning and taphonomy: high accuracy in the classification of cut marks made on fleshed and defleshed bones using convolutional neural networks. *Scientific Reports*, *9*(1), 1-12. https://doi.org/10.1038/s41598-019-55439-6

Ciudad Serrano, A., García Serrano, R., Caballero Klink, A., & Francia Villajos, A. (1983). Materiales paleolíticos de "El Sotillo". *Museo de Ciudad Real, Estudios y Monografías*, *8*.

Clark, T. R., Roff, G., Zhao, J., Feng, Y., Done, T. J., & Pandolfi, J. M. (2014). Testing the precision and accuracy of the U-Th chronometer for dating coral mortality events in the last 100 years. *Quaternary Geochronology*, *23*, 35-45. https://doi.org/10.1016/j.quageo.2014.05.002

Daura, J., Sanz, M., Arsuaga, J. L., Hoffmann, D. L., Quam, R. M., Ortega, M. C., Santos, E., Gómez, S., Rubio, A., & Villaescusa, L. (2017). New Middle Pleistocene hominin cranium from Gruta da Aroeira (Portugal). *Proceedings of the National Academy of Sciences*, *114*(13), 3397-3402. https://doi.org/10.1073/pnas.1619040114

de la Cruz, M. A. S. (2013). La delimitación del Campo de Montiel: principales enfoques y problemáticas. *Revista de Estudios Del Campo de Montiel*, *3*, 51-84.

de Lombera-Hermida, A., Bargalló, A., Terradillos-Bernal, M., Huguet, R., Vallverdú, J., García-Antón, M.-D., Mosquera, M., Ollé, A., Sala, R., & Carbonell, E. (2015). The lithic industry of Sima del Elefante (Atapuerca, Burgos, Spain) in the context of Early and Middle Pleistocene technology in Europe. *Journal of Human Evolution*, *82*, 95-106. https://doi.org/10.1016/j.jhevol.2015.03.002

Demuro, M., Arnold, L. J., Parés, J. M., Pérez-González, A., Ortega, A. I., Arsuaga, J. L., Bermúdez de Castro, J. M., & Carbonell, E. (2014). New luminescence ages for the Galería Complex archaeological site: resolving chronological uncertainties on the acheulean record of the Sierra de Atapuerca, Northern

Spain. *PLoS One*, *9*(10), e110169. https://doi.org/10.1371/journal.pone.0110169

Domínguez-Rodrigo, M., Cifuentes-Alcobendas, G., Jiménez-García, B., Abellán, N., Pizarro-Monzo, M., Organista, E., & Baquedano, E. (2020). Artificial intelligence provides greater accuracy in the classification of modern and ancient bone surface modifications. *Scientific Reports*, *10*(1), 1-11. https://doi.org/10.1038/s41598-020-75994-7

Domínguez-Solera, S. D., Moreno, D., & Pérez-Garrido, C. (2020). A new complete sequence from Lower to Middle Paleolithic: El Provencio complex (Cuenca, Spain). *Quaternary International*, *566*, 39-56. https://doi.org/10.1016/j.quaint.2020.04.053

Duval, M. (2015). Electron Spin Resonance Dating of fossil tooth enamel. In W. J. Rink & J. W. Thompson (Eds.), *Encyclopedia of Scientific Dating Methods* (pp. 239-246). Springer Netherlands. https://doi.org/10.1007/978-94-007-6304-3_71

Duval, M. (2018). Sobre el potencial de la resonancia paramagnética electrónica como herramienta geocronológica en contextos geoarqueológicos: un resumen de 30 años de investigación en la Península Ibérica. *Boletín Geológico y Minero*, *129*(1-2), 35-57. https://doi.org/10.21701/bolgeomin.129.1.002

Duval, M., & Grün, R. (2016). Are published ESR dose assessments on fossil tooth enamel reliable? *Quaternary Geochronology*, *31*, 19-27. https://doi.org/10.1016/j.quageo.2015.09.007

Duval, M., Grün, R., Parés, J. M., Martín-Francés, L., Campaña, I., Rosell, J., Shao, Q., Arsuaga, J. L., Carbonell, E., & Bermudez de Castro, J. M. (2018). The first direct ESR dating of a hominin tooth from Atapuerca Gran Dolina TD-6 (Spain) supports the antiquity of Homo antecessor. *Quaternary Geochronology*, *47*, 120-137. https://doi.org/10.1016/j.quageo.2018.05.001

Falguères, C., Bahain, J.-J., Pérez-González, A., Mercier, N., Santonja, M., & Dolo, J.-M. (2006). The Lower Acheulian site of Ambrona, Soria (Spain): ages derived from a combined ESR/U-series model. *Journal of Archaeological Science*, *33*(2), 149-157. https://doi.org/10.1016/j.jas.2005.07.006

Falguères, C., Bahain, J.-J., Yokoyama, Y., Arsuaga, J. L., Bermúdez de Castro, J. M., Carbonell, E., Bischoff, J. L., & Dolo, J.-M. (1999). Earliest humans in Europe: the age of TD6 gran Dolina, Atapuerca, Spain. *Journal of Human Evolution*, *37*(3-4), 343-352. https://doi.org/10.1006/jhev.1999.0326

Fernández Peris, J., Barciela, V., Blasco, R., Cuartero Monteagudo, F., & Sañudo Die, P. (2008). El Paleolítico Medio en el territorio valenciano y la variabilidad tecno-económica de la Cova del Bolomor. *Treballs d'arqueologia*, *14*, 141-169.

Fernández, V., Arteaga Cardineau, C., Baena Preysler, J., Escalante García, S., González Martín, J. A., López Recio, M., Marín Magaz, J. C., & Morín de Pablos, J. (2005). III. El Pleistoceno y las industrias paleolíticas de la cuenca alta y media del río Guadiana. In *Los primeros pobladores de Castilla-La Mancha* (pp. 142-190).

Ferràndez-Cañadell, C., Ribot, F., & Gibert, L. (2014). New fossil teeth of Theropithecus oswaldi (Cercopithecoidea) from the Early Pleistocene at Cueva Victoria (SE Spain). *Journal of Human Evolution*, *74*, 55-66. https://doi.org/10.1016/j.jhevol.2014.02.020

García-Martínez, D. (2019). ¿Dónde están los fósiles manchegos? El sesgo en el registro paleontológico del Pleistoceno de La Mancha. *Revista de Estudios Del Campo de Montiel*, *Extra 3*, 17-46. https://doi.org/10.30823/recm.02019116

García-Martínez, D., Valenciano, A., Suárez-Bilbao, A., Palancar, C. A., Megía García, I., Moreno, D., Campaña, I., & Moya-Maleno, P. R. (2020). New remains of a primitive badger from Cueva de los Toriles (Carrizosa, Castilla-La Mancha, Iberian Peninsula) suggest a new quaternary locality in the southern Iberian plateau. *Journal of Iberian Geology*. https://doi.org/10.1007/s41513-020-00127-y

García-Medrano, P., Ollé, A., Mosquera, M., Cáceres, I., & Carbonell, E. (2015). The nature of technological changes: The Middle Pleistocene stone tool assemblages from Galería and Gran Dolina-subunit TD10. 1 (Atapuerca, Spain). *Quaternary International*, *368*, 92-111. https://doi.org/10.1016/j.quaint.2015.03.006

García-Vadillo F.J., Duval M., Canals-Salomó A., Rodríguez-Álvarez X.-P., Garcia-Garriga J., Carbonell-Roura E. (2021). Contexto crono-estratigráfico y cultural del conjunto lítico de Base Menacho (cuenca del río Guadiana, Badajoz, España): primeros resultados. Cuaternario y Geomorfología 35 (3-4), pp. 147-173. https://doi.org/10.17735/cyg.v35i3-4.89904

Gibert, J., Gibert, L., Ribot, F., Ferràndez-Canadell, C., Sánchez, F., Iglesias, A., & Walker, M. J. (2008). CV-0, an early Pleistocene human pha-

lanx from Cueva Victoria (Cartagena, Spain). *Journal of Human Evolution*, *54*(1), 150-156. https://doi.org/10.1016/j.jhevol.2007.04.010

Gibert, J., & Pérez-Pérez, A. (1989). A human phalanx from the Lower Palaeolithic site of Cueva Victoria (Murcia, Spain). *Human Evolution*, *4*(4), 307-316. https://doi.org/10.1007/BF02437269

Gibert, L., Scott, G. R., Scholz, D., Budsky, A., Ferràndez, C., Ribot, F., Martin, R. A., & Lería, M. (2016). Chronology for the Cueva Victoria fossil site (SE Spain): evidence for early Pleistocene Afro-Iberian dispersals. *Journal of Human Evolution*, *90*, 183-197. https://doi.org/10.1016/j.jhevol.2015.08.002

González Martín, J. A. (2007). Presentación. Las tierras del Alto Guadiana: claves para interpretar su paisaje y algunos científicos que lo hicieron posible. *El Hombre y El Agua de Las Lagunas de Ruidera (Usos Históricos, Siglos XVI a Mediados Del XX)*, 15-53.

González Martín, J. A., Ordóñez, S., & García Del Cura, M. (1987). Evolución geomorfológica de las lagunas de Ruidera (Albacete-Ciudad Real). *Estudios Geológicos*, *43*, 227-239. https://doi.org/10.3989/egeol.87433-4592

González Martín, J. A., Ordóñez, S., & García del Cura, M. A. (2004). El alto Valle del Guadiana y las Lagunas de Ruidera. In G. Benito & J. Díez Herrero (Eds.), *Itinerarios geomorfológicos por Castilla La Mancha* (pp. 125-157). CSIC-SEG.

Goodfellow, I., Bengio, Y., & Courville, A. (2016). *Deep Learning. Massachusetts*. MIT press.

Grün, R. (2000a). An alternative model for open system U-series/ESR age calculations:(closed system U-series)-ESR, CSUS-ESR. *Ancient TL*, *18*, 1-4.

Grün, R. (2000b). Methods of dose determination using ESR spectra of tooth enamel. *Radiation Measurements*, *32*(5-6), 767-772. https://doi.org/10.1016/S1350-4487(99)00281-4

Grün, R. (2009). The DATA program for the calculation of ESR age estimates on tooth enamel. *Quaternary Geochronology*, *4*(3), 231-232. https://doi.org/10.1016/j.quageo.2008.12.005

Grün, R., & Brumby, S. (1994). The assessment of errors in past radiation doses extrapolated from ESR/TL dose-response data. *Radiation Measurements*, *23*(2-3), 307-315. https://doi.org/10.1016/1350-4487(94)90057-4

Grün, R., Eggins, S., Kinsley, L., Moseley, H., & Sambridge, M. (2014). Laser ablation U-series analysis of fossil bones and teeth. *Palaeogeography, Palaeoclimatology, Palaeoecology*, *416*, 150-167. https://doi.org/10.1016/j.palaeo.2014.07.023

Grün, R., & Katzenberger-Apel, O. (1994). An alpha irradiator for ESR dating. *Ancient TL*, *12*(2), 35-38.

Grün, R., Schwarcz, H. P., & Chadam, J. (1988). ESR dating of tooth enamel: coupled correction for U-uptake and U-series disequilibrium. *International Journal of Radiation Applications and Instrumentation. Part D. Nuclear Tracks and Radiation Measurements*, *14*(1-2), 237-241. https://doi.org/10.1016/1359-0189(88)90071-4

Guérin, G., Mercier, N., & Adamiec, G. (2011). Dose-rate conversion factors: update. *Ancient TL*, *29*(1), 5-8.

Hijano, C. F. (2013). Las Lagunas de Ruidera en los inicios de la Pequeña Edad del Hielo (siglo XVI). *Al-Basit: Revista de Estudios Albacetenses*, *58*, 37-73.

Jiménez Ramírez, S., & Chaparro Sabina, A. (1989). Las Lagunas de Ruidera en el tiempo. *Ciudad Real, Edición de Los Autores*.

Jordá Pardo, J. F. (2007). The wild river and the last Neanderthals: a palaeoflood in the geoarchaeological record of the Jarama Canyon (Central Range, Guadalajara province, Spain). *Geodinamica Acta*, *20*(4), 209-217. https://doi.org/10.3166/ga.20.209-217

Jordá Pardo, J. F. (2008). Yacimientos de vertebrados del Plioceno y Pleistoceno español. In Á. García Cortés, J. Águeda Villar, & J. Palacio Suárez-Valgrande (Eds.), *Contextos Geológicos Españoles. Una aproximación al patrimonio geológico español de relevancia internacional* (Vol. 1, pp. 171-183). Instituto Geológico y Minero de España.

Ketkar, N. (2017). Introduction to PyTorch. In *Deep learning with python* (pp. 195-208). Springer. https://doi.org/10.1007/978-1-4842-2766-4_12

Lisiecki, L. E., & Raymo, M. E. (2005). A Pliocene-Pleistocene stack of 57 globally distributed benthic δ18O records. *Paleoceanography*, *20*(1). https://doi.org/10.1029/2004PA001071

López-Recio, M., Morín de Pablos, J., Sánchez, F., Cuartero, F., Carrión, E., González Martín, J. A., Baena Preysler, J., Lázaro, A., Fernández, C., & Velázquez, R. (2001). Nuevos datos sobre la ocupación paleolítica en la cuenca media del río Guadiana (Ciudad Real). *Bolskan: Revista de Arqueología Del Instituto de Estudios Altoaragoneses*, *18*, 109-118.

López-Recio, M., Morín, J., Escalante, S., González, J.A., Baena, J., Carrión, E., Conde, C., Cuartero, F., Arteaga, C., Escolà, M., Fernández, C., Lázaro, A., Pérez-Juez, A., Regidor, D., Requejo, V., Sánchez, F., Velázquez, R. (2004). La ocupación paleolítica en Ciudad Real. Nuevos datos geomorfológicos y estratigráficos de las terrazas cuaternarias del río Guadiana. En: N. Bicho y A.F. Carvalho (Eds.), IV Congresso de Arqueología Peninsular (Vol. IV). Univerdad do Algarve, Faro, 303-309.

López Sanz, G. (1993). El acuífero 23 de la Mancha Occidental y el acuífero 24 del Campo de Montiel: Funcionamiento, Gestión, problemática y alternativas. *Universidad de Castilla-La Mancha. UCLM. Área de Economía Española e Internacional. Facultad de Ciencias Económicas y Empresariales (Albacete)*.

Lorenzo, C., Pablos, A., Carretero, J. M., Huguet, R., Vallverdú, J., Martinon-Torres, M., Arsuaga, J. L., Carbonell, E., & Bermudez de Castro, J. M. (2015). Early Pleistocene human hand phalanx from the Sima del Elefante (TE) cave site in Sierra de Atapuerca (Spain). *J Hum Evol*, *78*, 114-121. https://doi.org/10.1016/j.jhevol.2014.08.007

Ludwig, K. R. (2003). User's manual for Isoplot 3.00, a geochronological toolkit for Microsoft Excel. *Berkeley Geochronl. Cent. Spec. Publ.*, *4*, 25-32.

Marín Magaz, J. C. (2007). El hombre y el agua de las Lagunas de Ruidera. Usos históricos, siglos XVI a mediados del XX. *Tomelloso, Ediciones Soubriet*.

Marsh, R. E. (1999). *Beta-gradient isochrons using electron paramagnetic resonance: towards a new dating method in archaeology*. McMaster University.

Martín, J. A. G. (2000). Las transformaciones antrópicas del paisaje de los sistemas fluviales tobáceos del Centro de España. *Boletín de La Real Sociedad Española de Historia Natural. Sección Geológica*, *96*(1), 155-186.

Martínez-Navarro, B., Claret, A., Shabel, A. B., Perez-Claros, J. A., Lorenzo, C., & Palmqvist, P. (2005). Early Pleistocene "hominid remains" from southern Spain and the taxonomic assignment of the Cueva Victoria phalanx. *Journal of Human Evolution*, *48*(5), 517-523. https://doi.org/10.1016/j.jhevol.2005.02.003

Martínez-Navarro, B., Palmqvist, P., Shabel, A. B., Pérez-Claros, J. A., Lorenzo, C., & Claret, A. (2008). Reply to Gibert *et al*. (2008) on the supposed human phalanx from Cueva Victoria (Cartagena, Spain). *Journal of Human Evolution*, *54*(1), 157-161. https://doi.org/10.1016/j.jhevol.2007.09.011

Mazo, A. V. (1999). Vertebrados fósiles del Campo de Calatrava (Ciudad Real). *La Huella Del Pasado: Fósiles de Castilla-La Mancha (Aguirre, E. & Rábano, I., Eds.). Junta de Comunidades de Castilla La Mancha, Toledo*, 281-295.

Mazo, A. V., Pérez-González, A., & Aguirre, E. (1990). Las faunas pleistocenas de Fuensanta del Júcar y El Provencio y su significado en la evolución del Cuaternario de la Llanura manchega. *Boletín Geológico y Minero*, *101*(3), 404-418.

Megía García, I., Paulos-Bravo, R., Cifuentes-Alcobendas, G., Palancar, C. A., Suárez-Bilbao, A., Moya-Maleno, P. R., & García-Martínez, D. (2020). Typo-technological analysis of a bifacial stone tool from Cueva de los Toriles (Carrizosa, Castilla-La Mancha, Iberian Península) and its importance as a new Acheulean site from the Southern Iberian Plateau. *Proceedings of the European Society for the Study of Human Evolution*, 77.

Méndez-Quintas, E., Santonja, M., Pérez-González, A., Duval, M., Demuro, M., & Arnold, L. J. (2018). First evidence of an extensive Acheulean large cutting tool accumulation in Europe from Porto Maior (Galicia, Spain). *Scientific Reports*, *8*(1), 1-13. https://doi.org/10.1038/s41598-018-21320-1

Montero González, E. (2003). Geología, geomorfología e hidrogeología en las Lagunas de Ruidera. In *Lagunas de Ruidera: 25 años de Parque Natural* (Issue 10, pp. 34-37). Consejería de Medio Ambiente y Desarrollo Rural.

Moreno, D., Falguères, C., Pérez-González, A., Duval, M., Voinchet, P., Benito-Calvo, A., Ortega, A. I., Bahain, J.-J., Sala, R., & Carbonell, E. (2012). ESR chronology of alluvial deposits in the Arlanzón valley (Atapuerca, Spain): contemporaneity with Atapuerca Gran Dolina site. *Quaternary Geochronology*, *10*, 418-423. https://doi.org/10.1016/j.quageo.2012.04.018

Morín de Pablos, J., Recio, M. L., Gil, A. P., & García, S. E. (2007). El Reino de Don Quijote de La Mancha (Ciudad Real): un proyecto de gestión arqueológica. *Actas Del I Congreso de Patrimonio Histórico de Castilla-La Mancha: La Gestión Del Patrimonio Histórico Regional: Homenaje a Victoria Cabrera Valdés*, 177-188.

Moya-Maleno, P. R. (2011). ¿Caminante, no hay camino ...? Territorio y economía de la Edad del Bronce a través de los pasos tradicionales: el Campo de Montiel entre la Meseta Sur y la

Alta Andalucía. In *II Jornadas de Jóvenes en Investigación Arqueológica (Madrid, 6,7 y 8 de mayo de 2009)* (pp. 643-650).

Moyano, I. T., Barsky, D., Cauche, D., Celiberti, V., Grégoire, S., Lebegue, F., Moncel, M. H., & de Lumley, H. (2011). The archaic stone tool industry from Barranco León and Fuente Nueva 3, (Orce, Spain): Evidence of the earliest hominin presence in southern Europe. *Quaternary International*, *243*(1), 80-91. https://doi.org/10.1016/j.quaint.2010.12.011

Ollé, A., Mosquera, M., Rodríguez, X. P., de Lombera-Hermida, A., García-Antón, M. D., García-Medrano, P., Peña, L., Menéndez, L., Navazo, M., & Terradillos, M. (2013). The early and middle pleistocene technological record from Sierra de Atapuerca (Burgos, Spain). *Quaternary International*, *295*, 138-167. https://doi.org/10.1016/j.quaint.2011.11.009

Ordóñez, S., González Martín, J. A., García Del Cura, M. A., & Pedley, H. M. (2005). Temperate and semi-arid tufas in the Pleistocene to Recent fluvial barrage system in the Mediterranean area: The Ruidera Lakes Natural Park (Central Spain). *Geomorphology*, *69*(1-4), 332-350. https://doi.org/10.1016/j.geomorph.2005.02.002

Panera Gallego, J., Torres, T. de, Pérez-González, A., Ortiz Menéndez, J. E., Rubio Jara, S., & Uribelarrea del Val, D. (2011). *Geocronología de la terraza compleja de Arganda en el valle del río Jarama (Madrid, España)*. https://doi.org/10.3989/egeol.40550.204

Panera, J., Torres, T., Pérez-González, A., Ortiz, J. E., Rubio-Jara, S., & Uribelarrea del Val, D. (2011). Geocronología de la Terraza Compleja de Arganda en el valle del río Jarama (Madrid, España). *Estudios Geológicos*, *67*(2), 495-504. https://doi.org/10.3989/egeol.40550.204

Pérez-González, A., Parés, J. M., Carbonell, E., Aleixandre, T., Ortega, A. I., Benito, A., & Merino, M. Á. M. (2001). Géologie de la Sierra de Atapuerca et stratigraphie des remplissages karstiques de Galería et Dolina (Burgos, Espagne). *L'Anthropologie*, *105*(1), 27-43. https://doi.org/10.1016/S0003-5521(01)80004-2

Planchuelo, G. (1952). *Estudio del Alto Guadiana y de la altiplanicie del Campo de Montiel*. Universidad Complutense de Madrid.

Price, G. J., Feng, Y., Zhao, J., & Webb, G. E. (2013). Direct U-Th dating of vertebrate fossils with minimum sampling destruction and application to museum specimens. *Quaternary Geochronology*, *18*, 1-8. https://doi.org/10.1016/j.quageo.2013.07.003

Price, G. J., Ferguson, K. J., Webb, G. E., Feng, Y., Higgins, P., Nguyen, A. D., Zhao, J., Joannes-Boyau, R., & Louys, J. (2017). Seasonal migration of marsupial megafauna in Pleistocene Sahul (Australia-new Guinea). *Proceedings of the Royal Society B: Biological Sciences*, *284*(1863), 20170785. https://doi.org/10.1098/rspb.2017.0785

Querol, M. Á., & Santonja, M. (1983). La industria Achelense de El Martinete (Ciudad Real). *Homenaje al Prof. Martín Almagro Basch*, 83-93.

Ramírez, S. J., Sabina, A. C., & Alcolea Jiménez, J. J. (1982). El Paleolítico de Ruidera (Alto Guadiana). *Cuadernos de Estudios Manchegos*, *12*, 311-376.

Rodriguez-Hidalgo, A., Saladie, P., Olle, A., Arsuaga, J. L., de Castro, J. M. B., & Carbonell, E. (2017). Human predatory behavior and the social implications of communal hunting based on evidence from the TD10. 2 bison bone bed at Gran Dolina (Atapuerca, Spain). *Journal of Human Evolution*, *105*, 89-122. https://doi.org/10.1016/j.jhevol.2017.01.007

Rodriguez-Perez, F. J., Rosas, A., García-Martínez, D., Bastir, M., García-Tabernero, A., Estalrrich, A., Huguet, R., & Pastor, J. F. (2017). A 3D form comparative analysis of the Neandertal glenoid fossa in the context of the genus Homo. *Quaternary International*. https://doi.org/10.1016/j.quaint.2017.07.031

Rosas, A., & Bermudez de Castro, J. M. (1999). The ATD6-5 mandibular specimen from Gran Dolina (Atapuerca, Spain). Morphological study and phylogenetic implications. *Journal of Human Evolution*, *37*(3-4), 567-590. https://doi.org/10.1006/jhev.1999.0340

Rosas, A., Estalrrich, A., García-Tabernero, A., Bastir, M., García-Vargas, S., Sánchez-Meseguer, A., Huguet, R., Lalueza-Fox, C., Peña-Melián, Á., Kranioti, E. F., Santamaría, D., de la Rasilla, M., & Fortea, J. (2012). The Neandertals from El Sidrón (Asturias, Spain). Updating of a new sample, Les Néandertaliens d'El Sidrón (Asturies, Espagne). Actualisation d'un nouvel échantillon. *L'Anthropologie*, *116*(1), 57-76. http://www.scopus.com/inward/record.url?eid=2-s2.0-84857442771&partnerID=40&md5=be07d20a2e7eb6cfa5c08229d1d52609. https://doi.org/10.1016/j.anthro.2011.12.003

Rosas, A., Ferrando, A., Bastir, M., García-Tabernero, A., Estalrrich, A., Huguet, R., García-Martínez, D., Pastor, J. F., & de la Rasilla, M. (2017). Neandertal talus bones from El Sidrón site (Asturias, Spain): A 3D geometric mor-

phometrics analysis. *American Journal of Physical Anthropology*. https://doi.org/10.1002/ajpa.23280

Rosas, A., Martinez-Maza, C., Bastir, M., Garcia-Tabernero, A., Lalueza-Fox, C., Huguet, R., Ortiz, J. E., Julia, R., Soler, V., Torres, T. de, Martinez, E., Cañaveras, J. C., Sanchez-Moral, S., Cuezva, S., Lariol, J., Santamaria, D., de la Rasilla, M., & Fortea, J. (2006). Paleobiology and comparative morphology of a late Neandertal sample from El Sidrón, Asturias, Spain. *Proceedings of the National Academy of Sciences, USA*, *103*, 19266-19271. https://doi.org/10.1073/pnas.0609662104

Santisteban, J. I., & Schulte, L. (2007). Fluvial networks of the Iberian Peninsula: a chronological framework. *Quaternary Science Reviews*, *26*(22-24), 2738-2757. https://doi.org/10.1016/j.quascirev.2006.12.019

Santonja, M., Pérez-González, A., Domínguez-Rodrigo, M., Panera, J., Rubio-Jara, S., Sesé, C., Soto, E., Arnold, L. J., Duval, M., & Demuro, M. (2014). The Middle Paleolithic site of Cuesta de la Bajada (Teruel, Spain): a perspective on the Acheulean and Middle Paleolithic technocomplexes in Europe. *Journal of Archaeological Science*, *49*, 556-571. https://doi.org/10.1016/j.jas.2014.06.003

Santonja, M., Pérez-González, A., Villa, P., Soto, E., & Sesé, C. (2001). Elephants in the archaeological sites of Áridos (Jarama valley, Madrid, Spain). *La Terra Degli Elefanti. Consiglio Nazionale Delle Ricerche, Rome*, 602-606.

Santonja, M., Querol, M. A., & Peña, J. L. (1977). Aplicación de la tipología de industrias paleolíticas a la datación del Pleistoceno Superior en el Campo de Calatrava (Ciudad Real). In *Actas 2ª Reunión Nacional Grupo Español Trabajo Cuaternario. Trabajos sobre Neógeno-Cuaternario, Sección de Paleontología de Vertebrados y Humana, CSIC, Madrid, Vol. 6* (pp. 251-261).

Sesé, C. (2010). *Micromamíferos del yacimiento del Pleistoceno Medio de TAFESA (Madrid).*

Sesé, C., & Soto, E. (2002). Catálogo de los yacimientos de Vertebrados del Pleistoceno en las terrazas de los ríos Jarama y Manzanares. In J. Panera Gallego & S. Rubio Jara (Eds.), *Bifaces y Elefantes* (pp. 430-457). Museo Arqueológico regional.

Titton, S., Barsky, D., Bargalló, A., Serrano-Ramos, A., Vergès, J. M., Toro-Moyano, I., Sala-Ramos, R., Solano, J. G., & Jimenez Arenas, J. M. (2020). Subspheroids in the lithic assemblage of Barranco León (Spain): Recognizing the late Oldowan in Europe. *PloS One*, *15*(1), e0228290. https://doi.org/10.1371/journal.pone.0228290

Toro-Moyano, I., Martinez-Navarro, B., Agusti, J., Souday, C., Bermudez de Castro, J. M., Martinon-Torres, M., Fajardo, B., Duval, M., Falguères, C., Oms, O., Pares, J. M., Anadon, P., Julia, R., Garcia-Aguilar, J. M., Moigne, A. M., Espigares, M. P., Ros-Montoya, S., & Palmqvist, P. (2013). The oldest human fossil in Europe, from Orce (Spain). *J Hum Evol*, *65*(1), 1-9. https://doi.org/10.1016/j.jhevol.2013.01.012

Torres, T., & Mazo, A. V. (1991). El yacimiento Plioceno del Pozo de Piedrabuena (Campo de Calatrava, provincia de Ciudad Real). Geología, paleontología y análisis paleoambiental. *Estudios Geológicos*, *47*(5-6). https://doi.org/10.3989/egeol.91475-6428

Val, A., de la Peña, P., Bansal, S., Colino, F., Culey, J., Duval, M., Hodgskiss, T., Morrissey, P., Murray, A., Murungi, M., Neumann, F. H., Shadrach, K., Thomsen, K., van der Ryst, M., Witelson, D., & Stratford, D. (2021). The place beyond the trees: renewed excavations of the Middle Stone Age deposits at Olieboomspoort in the Waterberg Mountains of the South African Savanna Biome. *Archaeological and Anthropological Sciences*, *13*(7), 1-32. https://doi.org/10.1007/s12520-021-01302-7

Valdés, V. C. (1984). *El yacimiento de la Cueva de" El Castillo"(Puente Viesgo, Santander)* (Vol. 22). Editorial CSIC-CSIC Press.

Vallespí, E., Ciudad Serrano, A., & García Serrano, R. (1979). *Achelense y musteriense de Porzuna (Ciudad Real): Materiales de Superficie. Colección E. Oliver. Tomo I* (pp. 58-85).

Villa, P., & Mahieu, E. (1991). Breakage patterns of human long bones. *Journal of Human Evolution*, *21*(1), 27-48. https://doi.org/10.1016/0047-2484(91)90034-S

Walker, M. J., Ortega, J., López, M. v, Parmová, K., & Trinkaus, E. (2011). Neandertal postcranial remains from the Sima de las Palomas del Cabezo Gordo, Murcia, southeastern Spain. *American Journal of Physical Anthropology*, *144*(4), 505-515. https://doi.org/10.1002/ajpa.21428

Zhao, J., Yu, K., & Feng, Y. (2009). High-precision 238U-234U-230Th disequilibrium dating of the recent past: a review. *Quaternary Geochronology*, *4*(5), 423-433. https://doi.org/10.1016/j.quageo.2009.01.012

Recibido el 14 de julio de 2021
Aceptado el 3 de febrero de 2022